MAGNETO-TRANSPORT IN 2D MATERIALS

M.Sc. THESIS

Ву

Aman Kumar 2303151004



DEPARTMENT OF PHYSICS INDIAN INSTITUTE OF TECHNOLOGY INDORE MAY 2025

MAGNETO-TRANSPORT IN 2D MATERIALS

A THESIS

Submitted in partial fulfillment of the requirements for the award of the degree

of Master of Science

 $\mathbf{AMAN} \ \mathbf{KUMAR}$



DEPARTMENT OF PHYSICS INDIAN INSTITUTE OF TECHNOLOGY INDORE MAY 2025



INDIAN INSTITUTE OF TECHNOLOGY INDORE

CANDIDATE'S DECLARATION

I hereby certify that the work which is being presented in the thesis entitled Magneto-Transport in 2D Materials in the partial fulfillment of the requirements for the award of the degree of MASTER OF SCIENCE and submitted in the DEPARTMENT OF PHYSICS, Indian Institute of Technology Indore, is an authentic record of my own work carried out during the time period from August 2023 to May 2025 under the supervision of Prof. Preeti A. Bhobe, Head of Department, Department of Physics, IIT Indore.

The matter presented in this thesis has not been submitted by me for the award of any other degree of this or any other institute.

Signature of the student with date

(Aman Kumar)

This is to certify that the above statement made by the candidate is correct to the best of my/our knowledge.

Signature of the Supervisor of

 $\mathbf{M.Sc.} \ \mathbf{thesis} \ (\mathbf{with} \ \mathbf{date})$

(Prof. Preeti A. Bhobe)

Aman Kumar has successfully given his M.Sc. Oral Examination held on May 2025.

Convener, DPGC

Date: 20-05-25

Acknowledgements

I would like to sincerely thank my supervisor, Dr. Preeti Bhobe, for her constant guidance, encouragement, and patience throughout my MSc thesis. Her support not only helped me in shaping this work but also taught me how to approach research with curiosity and clarity.

I'm really grateful to my PhD seniors for their helpful suggestions and for always being there whenever I got stuck, whether in experiments or writing. A big thanks to my labmates too—for all the discussions, teamwork, and the good times in the lab that made even long hours enjoyable.

I thank IIT Indore and the Department of Physics for providing me with the opportunity and facilities to carry out my research. I'm especially thankful for access to the instruments and experimental setups that were crucial for my work in condensed matter physics.

Special thanks to the UGC-DAE CSR Mumbai Centre for allowing me to perform magnetoresistance measurements and for their technical support during my visit. This part of the project added a lot of value to my thesis.

Finally, I want to thank my friends for their constant support, motivation, and for keeping me sane through the ups and downs of this journey. I couldn't have done it without all of you.

Abstract

Two-dimensional (2D) materials have emerged as a fascinating platform for exploring novel electronic and transport phenomena, particularly in the presence of magnetic fields. These materials show exceptional electronic properties that provide insight into the band structure and quantities such as carrier mobility, fermi surface, and relaxation time, which are some key elements for understanding the transport properties of solids. To study the transport properties in 2D materials, we chose transition metal chalcogenides (TMC) particularly TiSe₂, ZrSe₂, and ZrSe₃ and prepared the single crystals of these materials in our laboratory using two-zone furnace. To confirm the purity of our samples, we carried out techniques such as X-ray spectroscopy, Raman spectroscopy, and Energy dispersive spectroscopy. We performed XRD to confirm the crystal structure, Raman for phase verification and EDS to confirm the composition of elements in our samples. We also carried out resistivity (ρ) vs temperature (T) measurement to investigate the electronic properties and, at last, we did magnetoresistance (MR) vs magnetic field (H) measurement to study and analyze the effect of magnetic field on the properties of the materials. From this we observed that TiSe₂ is very sensitive to its synthesis process and growth conditions, which can results in distinct properties, which we observed in our polycrystalline samples. Also, TiSe₂ showed properties like Charge Density Wave (CDW) and Metal-Insulator Transition (MIT) in its single crystal form. We also observed that ZrSe₂ shows metallic behavior in both polycrystalline and single crystal forms which directly contradicts its natural character, as it is a semiconductor by nature. These materials and the dependence of their properties on the surrounding can provide some exceptional information about their electronic properties and can help us to understand their behavior in different external conditions.

Contents

A	Acknowledgements			2
Abstract				3
1	Introduction			10
	1.1	Transp	port Phenomena in Solids	11
		1.1.1	The Boltzmann Transport Equation	12
	1.2	Magne	etoresistance	13
		1.2.1	Types of MR	14
	1.3	Charge	e Density Wave (CDW)	15
		1.3.1	The Formation Mechanism of CDW	16
	1.4	Weak	Localization	17
2	Experimental Methods			19
	2.1	Synthe	esis Methods	19
		2.1.1	Chemical Vapour Transport Method	19
		2.1.2	Solid State Method	20
	2.2	Chara	cterization Techniques	21
		2.2.1	X-Ray Diffraction (XRD)	21
		2.2.2	Raman Spectroscopy	23
		2.2.3	Scanning Electron Microscopy with Energy-Dispersive X-ray Spectroscopy	
			(SEM-EDXS)	25
	2.3	Measu	rement System	27

		2.3.1	Closed Cycle Refrigerator System	27
		2.3.2	Current Source	29
		2.3.3	Voltmeter	30
		2.3.4	Temperature Controller	30
	2.4	Physic	cal Property Measurement System (PPMS)	30
3	Ch	aracte	rization Results	32
	3.1	Mater	ial : $TiSe_2$	32
		3.1.1	Synthesis of Single Crystals by CVT Method	32
		3.1.2	Synthesis of Polycrystalline by Solid State Method	33
		3.1.3	XRD pattern, Raman Spectra and EDS data of TiSe_2	33
	3.2	Mater	ial : $\mathbf{Zr}_{0.05}\mathbf{Ti}_{0.95}\mathbf{Se}_{2}$	35
		3.2.1	Single Crystals by CVT Method	35
		3.2.2	XRD pattern, Raman Spectra and EDS data of $\mathrm{Zr}_{0.05}\mathrm{Ti}_{0.95}\mathrm{Se}_2.$	36
4	Ele	ectroni	c Properties	38
	4.1	Mater	$ial: TiSe_2 \dots \dots$	38
		4.1.1	Introduction	38
		4.1.2	Resistivity vs Temperature Measurement	39
	4.2	Mater	$\mathrm{ial}: \mathrm{Zr}_{0.05}\mathrm{Ti}_{0.95}\mathrm{Se}_{2} \ \ldots \ldots \ldots \ldots \ldots \ldots \ldots \ldots$	41
		4.2.1	Introduction	41
		4.2.2	Resistivity vs Temperature Measurement	42
		4.2.3	$\mathrm{MR}(\%)$ Vs Magnetic Field	43
	4.3	Mater	$\mathrm{ial}: \mathrm{ZrSe}_2 \ldots \ldots \ldots \ldots \ldots$	44
		4.3.1	Introduction	44
		4.3.2	Resistivity vs Temperature Measurement	44
	4.4	Mater	ial : $ZrSe_3$	46
		4.4.1	Introduction	46
		4.4.2	Resistivity vs Temperature Measurement	46
		443	MR(%) Vs Magnetic Field	47

5 Conclusion 49

List of Figures

1.1	Types of 2D materials. [1]	10
1.2	A band gap diagram showing the different sizes of band gaps for conductors,	
	semiconductors, and insulators. [2]	12
1.3	Anisotropic MR data of a Permalloy material. [17]	14
1.4	Illustration of band structure before and after phase transition. [4]	15
1.5	Schematic illustrating the basic physics of weak localization. [12]	18
2.1	Schemetic of CVT experiments	20
2.2	The fig. shows Two-zone furnace, Muffle furnace, Hydraulic press, Vacuum Seal-	
	ing system, Glove box, and mortar-pestle	20
2.3	X-Ray Spectrum of a tungsten tube. [6]	21
2.4	Bruker-D2-Phaser X-ray diffractometer	22
2.5	Energy diagram for light scattering. [7]	23
2.6	Layout of a Raman Spectrometer.[8]	24
2.7	HORIBA LabRam HR Evolution Raman Spectrometer	24
2.8	Rays and electrons formed as a result of the interaction of the incoming electron	
	beam. [9]	25
2.9	Characteristic X-ray emission from an atom. [10]	26
2.10	JSM-7610FPlus Schottky Field Emission Scanning Electron Microscope	26
2.11	Resistivity Measurement System in our QMM lab	27
2.12	Schematic of the Janis CCR System	28
2.13	Schematic of the Cold Head.	29
2 14	Image of an PPMS	31

3.1	Images of single crystal of TiSe ₂ grown in our LTP lab	32
3.2	Polycrystal sample of TiSe ₂	33
3.3	XRD pattern of TiSe ₂	34
3.4	Raman spectra of TiSe ₂	34
3.5	Chemical Composition of TiSe ₂	35
3.6	Images of single crystal of $Zr_{0.05}Ti_{0.95}Se_2$ grown in our LTP lab	36
3.7	XRD pattern of $Zr_{0.05}Ti_{0.95}Se_2$	36
3.8	Raman spectra of ${\rm Zr_{0.05}Ti_{0.95}Se_2}$ compared with the raman spectra of ${\rm TiSe_2}$	37
3.9	Chemical composition of $Zr_{0.05}Ti_{0.95}Se_2$	37
4.1	ρ -T plot of polycrystalline samples of TiSe ₂ . Here, red line and blue line represents	
	sample 1 and sample 2 respectively	39
4.2	ρ -T plot of TiSe ₂ single crystal	40
4.3	The derivative of the resistivity plotted as a function of temperature	41
4.4	Resistivity Measurement of $Zr_{0.05}Ti_{0.95}Se_2$ polycrystalline sample	42
4.5	Magnetoresistance vs Magnetic field plot of $\rm Zr_{0.05}Ti_{0.95}Se_2$ at temperatures- 10 K	
	and 300 K	43
4.6	Resistivity (ρ) vs Temperature (T) plot of ZrSe ₂ . The red line is fitted to Eq.	
	(4.1) and the blue line is fitted to Eq. (4.2)	45
4.7	Resistivity (ρ) vs Temperature (T) plot of ZrSe ₃ . The red and blue lines represents	
	the warming and cooling of samples during the measurement	46
4.8	Magnetoresistance vs Magnetic field plot of $\rm ZrSe_3$ at temperatures- 200 K and	
	300 K	47

List of Tables

3.1	EDS Analysis Results	35

Chapter 1

Introduction

Since their introduction to the field of physics and material science, Two-Dimensional Materials have revolutionized the area of research, unfolding new concepts and theories. With a thickness of one or two atoms with strong covalent bonds within the plane and weak Van der Waals interaction between its layers, they simultaneously exhibit properties that can be significantly different from their bulk counterparts. Having such a small size and distinct properties, they pave the way for new technological advancements.

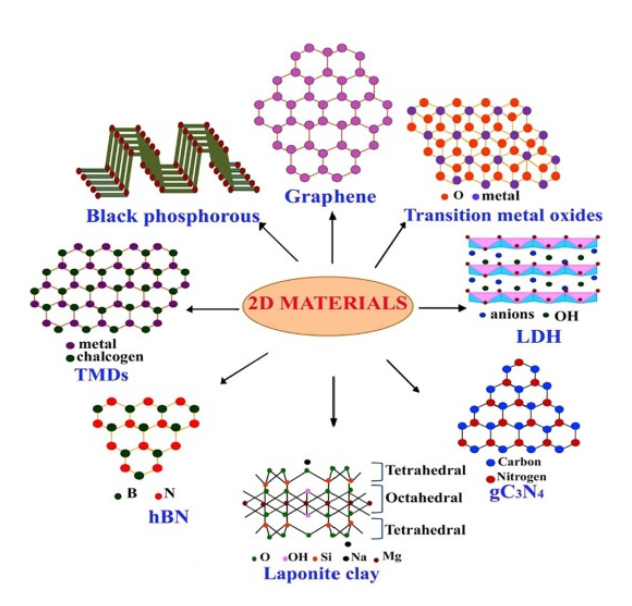


Figure 1.1: Types of 2D materials. [1]

Transition Metal Chalcogenides (TMCs), one of the type of 2D materials, have attracted significant interest because of their compelling physical, chemical, and optical properties. The transport properties of these materials have special significance as, through intercalation and

doping, their properties can be modified, providing us with additional information about their crystal structures. TiSe₂, one of the TMDC, shows a $(2 \times 2 \times 2)$ CDW transition at low temperatures that results in periodic modulations of the electronic charge density and Metal-Insulator transition due to temperature-dependent carrier concentration. Similarly, ZrSe₂, a semiconductor, shows metallic-type behavior in its resistivity measurements because of some defects or deep traps. In TMDCs, the presence of strong electron correlations and spin-orbit coupling complicates the transport behavior which can lead to unconventional properties such as weak localization, and the kondo effect.

1.1 Transport Phenomena in Solids

Solids are defined primarily in three categories: Metals, Semiconductors, and Insulators. There is another type in between metals and semiconductors, known as Semimetals. Metals show high charge-transport properties as the conduction band (CB) and valence band (VB)overlap each other. Metals follow the Fermi-Dirac distribution function to fill the quantum states. Electrons in metals can travel from the VB to CB with the slightest disturbance in their surroundings. An intrinsic semiconductor has no charge carriers at zero kelvin (T = 0) and therefore there is no transport of carriers under any external fields. At T \neq 0, there are some thermally generated carriers that serve in the transport in semiconductors. Insulators, on the other hand, have very little charge transport; hence, the transport happens possibly because of some defects or the ions that can participate in the transport of charge carriers under the influence of external fields. Talking about semimetals, the conduction and valence bands in these materials, either slightly overlap or touch each other at discrete points in momentum space. The properties of semimetals lies in between metals and semiconductors, making them a potential candidate for the research.

To study the transport in solids, two major quantities that almost describe charge transport are carrier mobility and carrier density. Electrical conductivity depends on the product of these two quantities. Carrier density and carrier type can be determined using the Hall effect, and carrier mobility can be determined by using the results of magnetoresistance measurements.

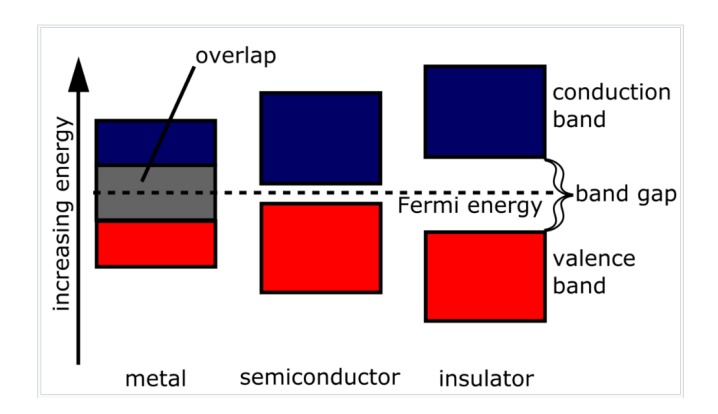


Figure 1.2: A band gap diagram showing the different sizes of band gaps for conductors, semi-conductors, and insulators. [2]

1.1.1 The Boltzmann Transport Equation

The Boltzmann Transport Equation (BTE) is a fundamental equation in condensed matter physics that is used to describe transport in materials. It explains how charge carriers (electrons and holes) move and scatter in a material under external forces (electric and magnetic fields).

According to this equation, in the steady state, the change in the distribution function $f(\mathbf{r}, \mathbf{k}, t)$ which determines the probability of finding an electron at position \mathbf{r} , crystal momentum \mathbf{k} , and time t corresponds to no net change. Therefore, the change in $f(\mathbf{r}, \mathbf{k}, t)$ due to the three processes namely diffusion, the effect of forces and fields, and collisions, results in zero. [11]

$$\frac{\partial f(\mathbf{r}, \mathbf{k}, t)}{\partial t} \bigg|_{diffusion} + \frac{\partial f(\mathbf{r}, \mathbf{k}, t)}{\partial \mathbf{t}} \bigg|_{fields} + \frac{\partial f(\mathbf{r}, \mathbf{k}, t)}{\partial t} \bigg|_{collisions} = 0.$$
(1.1)

We can solve the Boltzmann equation using two approximations:

1. Assuming the perturbation due to external fields and forces to be small enough so that the distribution function can be linearized and written as:

$$f(\mathbf{r}, \mathbf{k}) = f_0(E) + f_1(\mathbf{r}, \mathbf{k}) \tag{1.2}$$

where, $f_0(E)$ is the equilibrium distribution function (the fermi function) which depends only on the energy E, while $f_1(\mathbf{r}, \mathbf{k})$ is the perturbation term representing the departure from equilibrium.

2. The collision term in the Boltzmann equation is written in the relaxation time approxima-

tion so that the system returns to equilibrium uniformly:

$$\left. \frac{\partial f}{\partial t} \right|_{collisions} = -\frac{(f - f_0)}{\tau} = -\frac{f_1}{\tau}$$
 (1.3)

where $\tau = \tau(\mathbf{k})$ denotes Relaxation time describes how long it takes for a material to return to its normal, balanced state after an external influence—like an electric field or a temperature difference—is removed. It can vary depending on the crystal momentum, which means that different electrons in the material can relax back to equilibrium at different rates depending on how they're moving through the crystal.

When the fields are turned off at t=0, leads to the solutions of equation to.

$$f(t) = f_0 + [f(0) - f_0]e^{-t/\tau}$$
(1.4)

where, f_0 is the equilibrium distribution and f(0) is the distribution function at time t=0.

With these approximations, the Boltzmann equation is solved to find the distribution function, which in turn determines the number density and current density. The current density is given by

$$\mathbf{j}(\mathbf{r},t) = \frac{e}{4\pi^3} \int \mathbf{v}(\mathbf{k}) f(\mathbf{r}, \mathbf{k}, t) d^3k$$
 (1.5)

and the carrier density is given by

$$\mathbf{n}(\mathbf{r},t) = \frac{1}{4\pi^3} \int f(\mathbf{r}, \mathbf{k}, t) d^3k$$
 (1.6)

where, d^3k is an element of 3D wavevector space.

1.2 Magnetoresistance

It refers to the change in electrical resistance of a solid material when subjected to an external magnetic field. The effect is observed in various materials, including metals, semiconductors, and complex oxides. When a metal is subjected to a steady, uniform magnetic field, its resistivity changes depending on various factors such as the choice of material, direction of magnetic field

and current, and strength of magnetic field.

MR % is calculated by the following the formula

$$MR\% = \frac{[\rho(H) - \rho(0)]}{\rho(0)} \times 100 \tag{1.7}$$

1.2.1 Types of MR

There are several types of magnetoresistance, each with unique characteristics and underlying mechanisms:

- 1. Ordinary Magnetoresistance (OMR): OMR is the basic form of MR arises from the lorentz force acting on charge carriers (electrons and holes), causing them to follow curved paths in a magnetic field. The curvature of the charge carriers' trajectories increases the effective path length, leading to increased scattering and, consequently, to higher resistance.
- 2. Anisotropic Magnetoresistance (AMR): AMR is observed in ferromagnetic materials and depends on the relative orientation between the current and the magnetization of the material. The resistance change occurs due to spin-orbit coupling, which causes the scattering of charge carriers to depend on their spin orientation relative to the magnetization direction.

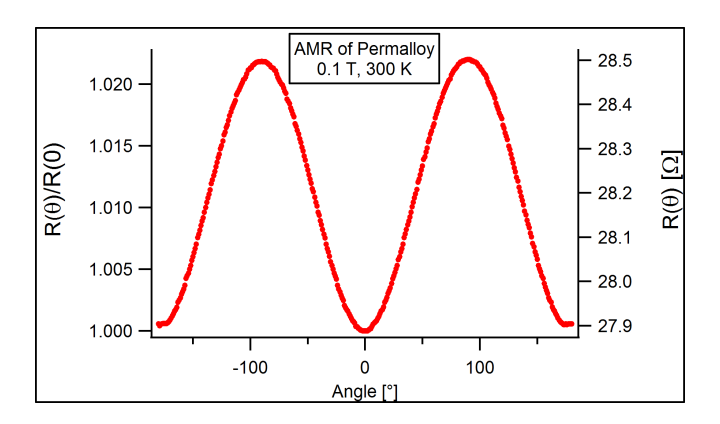


Figure 1.3: Anisotropic MR data of a Permalloy material. [17]

3. Giant Magnetoresistance (GMR): GMR is a large change in resistance observed in thin film structures composed of alternating ferromagnetic and non-magnetic layers.

- 4. Tunnel Magnetoresistance (TMR): TMR occurs in magnetic tunnel junctions, where two ferromagnetic layers are separated by an insulating barrier.
- 5. Colossal Magnetoresistance (CMR): The mechanism of CMR is complex and involves a combination of double exchange interactions, charge ordering, and phase separation phenomena.

1.3 Charge Density Wave (CDW)

It is a fascinating quantum phenomenon that emerges in certain low-dimensional materials because of their unstable structure at low temperatures. According to Peierls' theory, at low temperatures, the crystal structures of 1D metallic systems are prone to periodic distortions, modulating the electronic charge density, resulting in the formation of CDW phase. They are collective electronic states characterized by periodic modulations in the charge density of a material, often accompanied by distortions in the underlying crystal lattice.

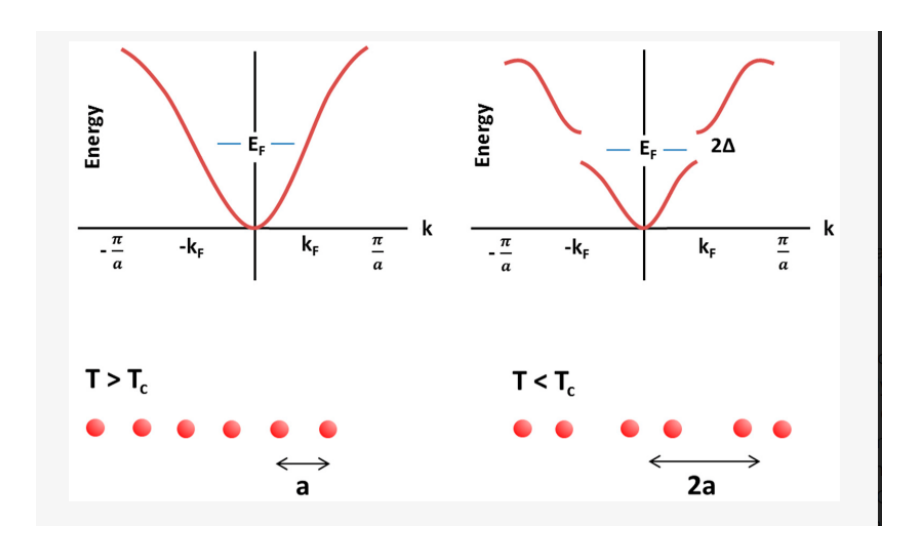


Figure 1.4: Illustration of band structure before and after phase transition. [4]

In a one-dimensional (1D) metal, atoms are arranged in a regular chain with equal spacing defined by the lattice constant a. Electrons fill energy levels from low to high, and if we assume there's one electron per atom, the system is half-filled. In this case, the Brillouin zone spans from $-\pi/a$ to $+\pi/a$, and the Fermi level lies at $K_F = \pm \pi/2a$. At this stage, the system is in its metallic ground state.

However, 1D systems are unstable at low temperatures, and even small changes in the environment can cause the atomic lattice to distort. One common type of distortion is dimerization, where every two neighboring atoms pair up to form a new unit cell. This doubles the spacing between repeating units to 2a, shifting the boundary of the Brillouin zone to $\pm \pi/2a$. Now, since there's still one electron per atom, the band becomes completely filled, and the system transitions from a metal to an insulator.

This transition happens because the charge density modulation has a wavevector $q = 2K_F$, which matches the new Brillouin zone boundary. This causes an energy gap to open at the Fermi level $(K_F = \pm \pi/2a)$, leading to a more stable, lower-energy state. The energy saved by opening this gap is greater than the energy cost of distorting the lattice, so the system naturally shifts to this new state.

In an ideal, undisturbed lattice at low temperatures, such distortions occur due to interactions between electrons and collective excitations, resulting in a charge density wave (CDW)—a periodic modulation of electron density that goes hand-in-hand with the lattice distortion and transforms the system into an insulating state.

When a lattice distortion happens, it can change the size of the unit cell, meaning the new lattice constant, a', might not be exactly twice the original (2a), and the ratio a'/a can vary. If this ratio is a rational number (like 2, 3/2, etc.), the CDW is called commensurate—meaning it fits neatly with the original lattice. But if the ratio is an irrational number (like π), the CDW is called incommensurate, meaning it doesn't align perfectly with the original lattice structure.

1.3.1 The Formation Mechanism of CDW

There are mainly four formation mechanisms that results in CDW in any material:

1. Fermi Surface Nesting Mechanism: Fermi surface nesting is a phenomenon where part of the Fermi surface overlaps with another part when shifted by a specific wave vector, known as the nesting vector (q). This overlap leads to strong interactions between electrons and phonons (vibrations in the lattice) at the Fermi surface. As a result, the phonons become unstable, and their vibration frequencies drop sharply and abruptly. This

instability causes the crystal lattice to distort, which then leads to a rearrangement of the atoms and the distribution of electrons in the material.

- 2. Electron Phonon Coupling Mechanism: Inelastic scattering occurs between electrons and phonons away from the Fermi surface. As the temperature rises, the number of phonons increases, leading to more frequent scattering of electrons by these phonons.
- 3. **Electron-Electron Interaction:** In more delocalized (dispersed) systems, electron-electron interactions become stronger. When these interactions dominate, the system can exhibit multiple possible ground states—some of which are believed to be associated with charge density wave (CDW) formation.
- 4. **Jahn Teller Effect**: The transition is driven by structural distortions that break the degeneracy of the ground state energy, because of distortion the systems energy gets lower.

1.4 Weak Localization

Weak Localization is a quantum correction to the classical conductivity in disordered materials. According to the Drude model (classical theory), electrons are like gas particles that move freely in random directions with some momentum. They occasionally scatter from ion cores and lose their momentum. The average time between two collisions is represented by relaxation time. Conductivity is given by

$$\sigma = \frac{ne^2\tau}{m^*} \tag{1.8}$$

Here we assume that no quantum effects are applicable. This mostly works at high temperatures where quantum effects averages out.

At low temperatures or in disordered materials, we consider the wave nature of electrons. So, electrons have a wave function with an amplitude and a phase. Electrons can interfere with themselves due to superposition of paths. These interference effects leads to slight deviation from drude model. It modifies the classical conductivity equation which now be represented as

$$\sigma = \sigma_{Drude} + \Delta \sigma_{WL} \tag{1.9}$$

where,

$$\Delta \sigma_{WL} = \frac{-e^2}{2\pi^2 \hbar} log(\frac{\tau_{\phi}}{\tau}) \tag{1.10}$$

In a disordered system, electrons can scatter off from impurities and some electrons can head back to their origin creating a loop path. Now those electrons create a quantum interference between the clockwise and counter-clockwise paths. If electron's phase coherence is preserved along both the paths, then the interference is constructive, which increases the probability that the electron stays near the origin and its forward motion is blocked. This reduces the conductivity because it enhances backscattering.

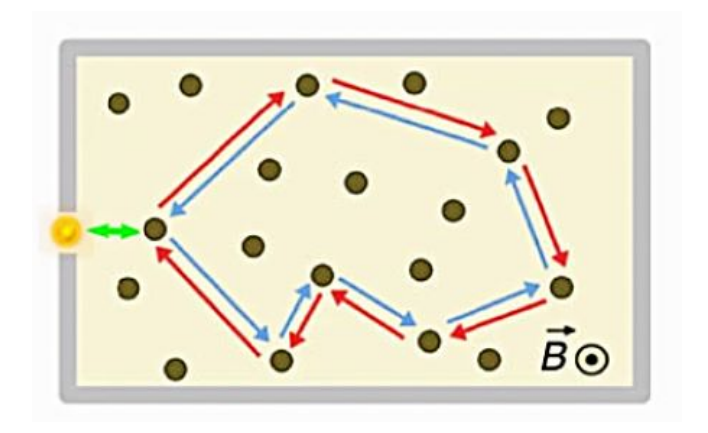


Figure 1.5: Schematic illustrating the basic physics of weak localization. [12]

For weak localization to happen, there is a necessary condition that should be satisfied. The phase coherence time (τ_{ϕ}) should be greater than the momentum relaxation time (τ) . Also, the electrons must undergo multiple scattering events and it must maintain its quantum phase coherence over those scatterings so that interference can happen.

Chapter 2

Experimental Methods

2.1 Synthesis Methods

For the preparation of either a single crystal or a polycrystal, we followed a defined procedure which includes: weighing of the elements according to the stoichiometry. Then we need to mix them properly by grinding them in mortar-pestle in a glove box with argon atmosphere. After that, the obtained mixed powder was pressed into a circular pellet using the hydraulic press and was sealed in a quartz tube under a vaccum of 8×10^{-5} mbar. The vacumm quartz tube was placed into a furnace (Two -zone furnace for single crystal and Muffle furnace for polycrystal) and heated according to the temperature needed for the synthesis. For the synthesis, we follow two methods: Chemical vapour transport method and Solid state method. We have discussed the above methods in detail below:

2.1.1 Chemical Vapour Transport Method

This method uses the reactions to form crystals. It consists of a transporting agent, which deposits the reactants in the form of crystals somewhere else. It is based on the fact that a solid (a condensed phase), has an insufficient pressure for its own volatilization. But the pertinent phase can be volatilized in the presence of a gaseous reactant (the transport agent). For the deposition, it require different external conditions, usually different temperatures, at the position of crystallization than at the position of volatilization. This technique requires a Two-Zone

Furnace to maintain different temperatures at the two ends known as hot end and cold end. The Hot end refers to the position of volatilization where the transporting agent and the elements react with each other, and the temperature at this end is higher as compare to the other end, while the Cold end refers to the position of crystallization, where the transporting agent deposits the sample in the form of crystals. [5]

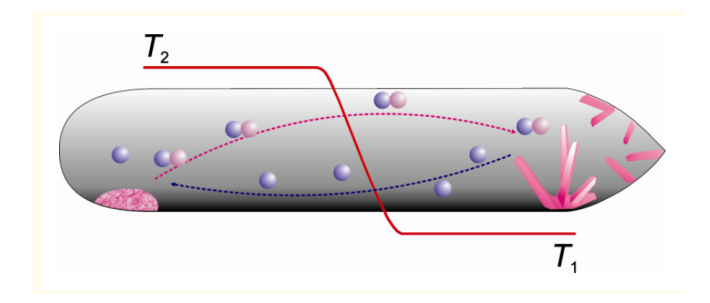


Figure 2.1: Schemetic of CVT experiments.

2.1.2 Solid State Method

This is the simplest and most commonly used method for synthesizing materials in material science. It involves directly reacting solid starting materials at high temperatures. The elemental powders are carefully weighed based on the stoichiometric ratios from the reaction equation and then thoroughly ground in an agate mortar to achieve the desired phase. After that, the mixture is heated under controlled conditions to help form well-defined crystalline structures.



Figure 2.2: The fig. shows Two-zone furnace, Muffle furnace, Hydraulic press, Vacuum Sealing system, Glove box, and mortar-pestle.

2.2 Characterization Techniques

After synthesizing the samples, we need to perform different characterization techniques to authenticate the quality of our samples. For phase identification and to analyze the crystal structure, we performed X-ray diffraction spectroscopy on our material samples, similarly, to study vibrational properties, we used Raman spectroscopy and to find the composition of the elements in our samples, we performed Energy-dispersive X-ray spectroscopy. For the resistivity measurement, we used Closed Cycle Refrigerator (CCR) and other electronic instruments. These all are discussed in detail below.

2.2.1 X-Ray Diffraction (XRD)

X-ray diffraction (XRD) is a powerful and non-destructive method used to study different properties of materials. It can help identify the phases present in a material, its crystal structure, texture, and more. This technique works on different types of samples—powders, solids, and even liquids. X-rays themselves are a type of electromagnetic wave, with wavelengths and energies lies between those of gamma rays and ultraviolet light.

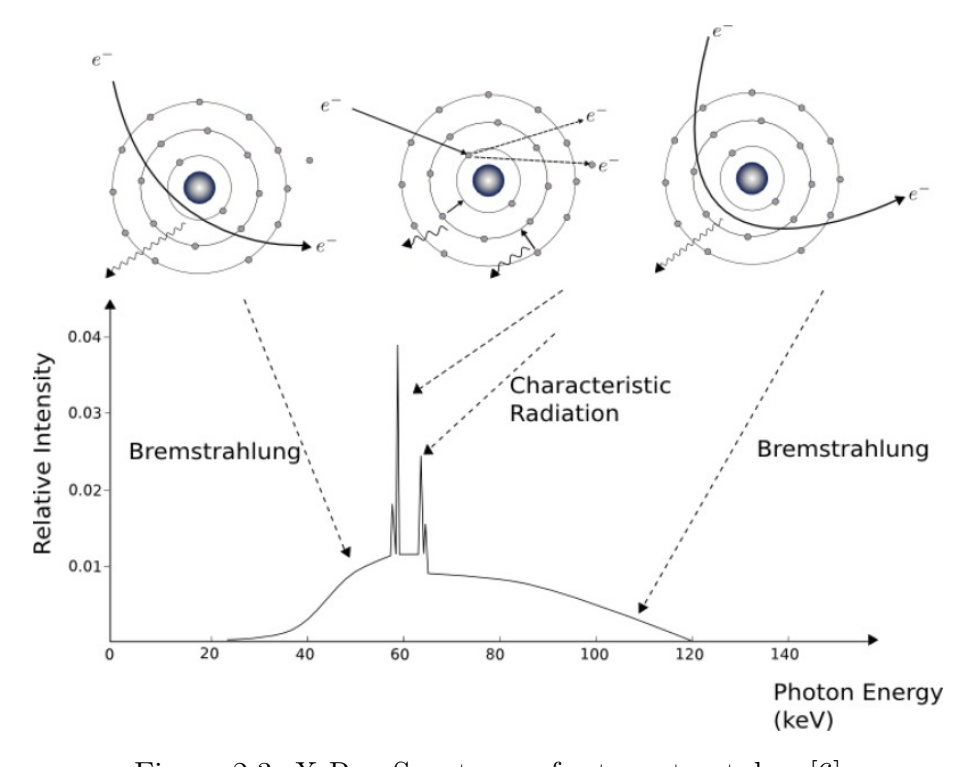


Figure 2.3: X-Ray Spectrum of a tungsten tube. [6]

There are a few ways to generate X-rays strong enough for diffraction studies. The most common methods include hitting a metal target (called the anode) with a focused beam of electrons, and using electromagnetic fields to bend high-energy electrons, which causes them to release X-rays.

When X-rays are produced, they come in two main types: continuous and characteristic. Continuous X-rays happen when fast-moving charged particles (like electrons) suddenly slow down or stop. This type of radiation is known as Bremsstrahlung." On the other hand, characteristic X-rays are produced when an electron from an outer shell falls into an empty spot in one of the atom's inner shells. This releases energy in the form of X-rays that are unique to each element, kind of like a fingerprint.

In X-ray powder diffraction, the sample is made up of a large number of tiny crystals (called crystallites) that are ideally oriented in random directions. Because all possible orientations are present, we only need to change the angles at which the X-rays hit and leave the sample. The instrument records how much X-ray intensity is detected at different angles, and this data is used to create a pattern called a diffractogram. The X-rays are diffracted (bent) by the different phases in the sample, pass through more optical parts, and finally reach the detector. By changing the angle between the incoming and outgoing X-rays (called 2θ), we can measure the intensity at each angle and build the diffractogram.

For our experiment, we used a Bruker D2-Phaser X-ray diffractometer to study the phases present in our polycrystalline samples.

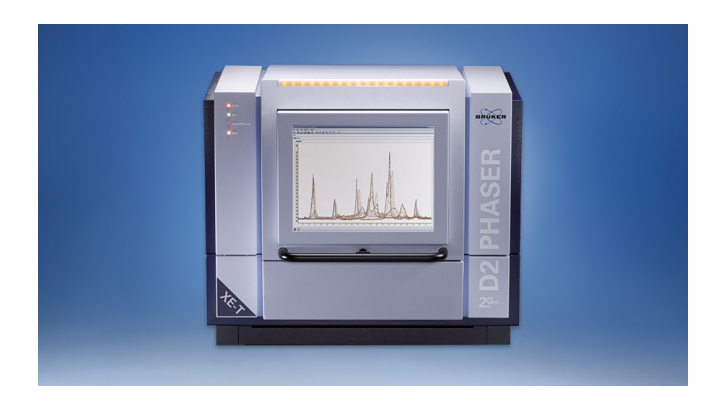


Figure 2.4: Bruker-D2-Phaser X-ray diffractometer.

2.2.2 Raman Spectroscopy

Raman spectroscopy is a powerful, non-destructive technique used to study vibrations and other low-energy motions in materials. It works by shining light on a sample and analyzing how some of the scattered light changes in energy. This energy shift happens because the light interacts with vibrations within the molecules. Raman scattering occurs when a vibration in a molecule changes how easily its electron cloud can be distorted—this property is called polarizability. For a vibration to be detected in Raman spectroscopy (called Raman-active), it must cause a change in polarizability during the vibration.

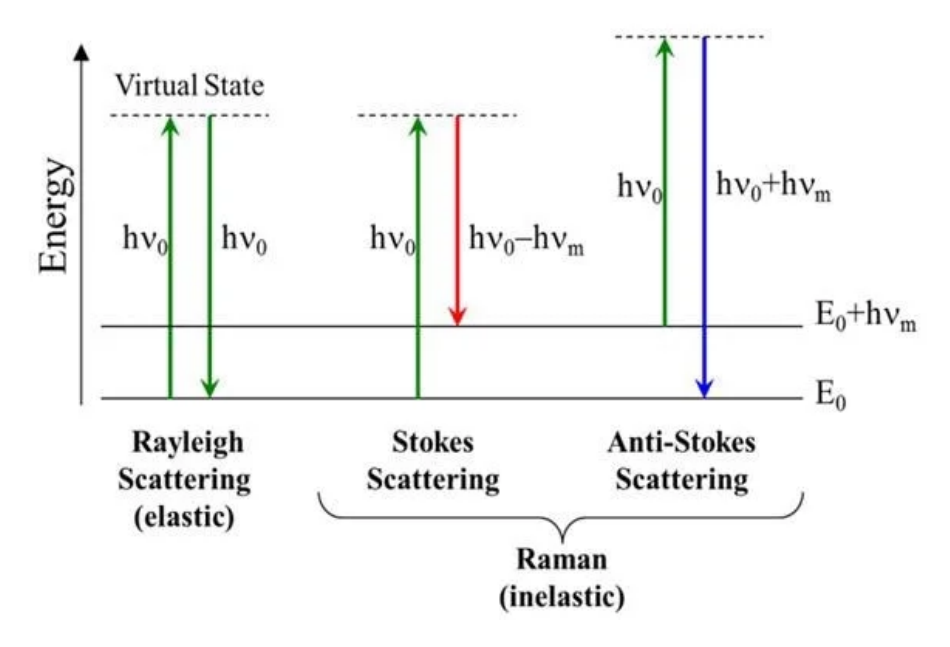


Figure 2.5: Energy diagram for light scattering. [7]

When monochromatic light (like a laser) shines on the surface of a sample, most of the light is scattered without any change in energy—this is known as elastic scattering or Rayleigh scattering. However, a small portion of the light interacts with the molecular vibrations in the material, causing a change in the energy of the scattered photons. This is called inelastic scattering, or Raman scattering. This appears as a series of peaks in the spectrum, shifted to both lower and higher frequencies relative to the original (Rayleigh) peak. The lower-frequency shifts are called Stokes lines, while the higher-frequency shifts are known as anti-Stokes lines. Since Stokes lines are typically much stronger, Raman spectra usually focus on them for analysis.

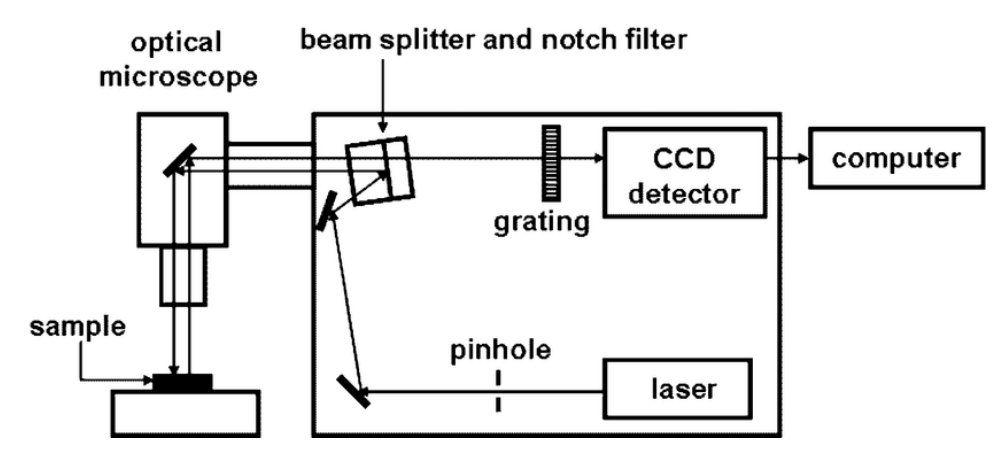


Figure 2.6: Layout of a Raman Spectrometer.[8]

In a Raman experiment, monochromatic light is focused onto the sample, usually from a laser. The light that scatters off the sample at a right angle (90°) is collected and passed through a high-resolution device called a monochromator, which separates the light based on its energy.

The laser's wavelength stays constant, but the scattered light may have slightly different energies. By measuring these energy differences, we get a Raman spectrum, which shows the intensity of scattered light versus the Raman shift. This spectrum tells us about the vibrational modes of the molecules or crystal structure in the material. Each material produces a unique pattern of peaks in its Raman spectrum, such as a fingerprint, which helps us identify what the material is.

For our samples, We used HORIBA LabRam HR Evolution raman spectrometer.



Figure 2.7: HORIBA LabRam HR Evolution Raman Spectrometer.

2.2.3 Scanning Electron Microscopy with Energy-Dispersive X-ray Spectroscopy (SEM-EDXS)

Energy Dispersive X-ray Spectroscopy (EDS) is a micro-analysis technique used to find out what elements are present in a sample. It is often used in conjunction with scanning electron microscopy (SEM), which is a method used to study the surface structure and composition of materials. SEM works by using a focused beam of high-energy electrons that scans the surface of a solid sample. When these electrons hit the sample, they interact with it and produce different types of signals. These signals give us information about the surface shape (morphology), the elements present (composition), and the arrangement and orientation of the crystals in the material.

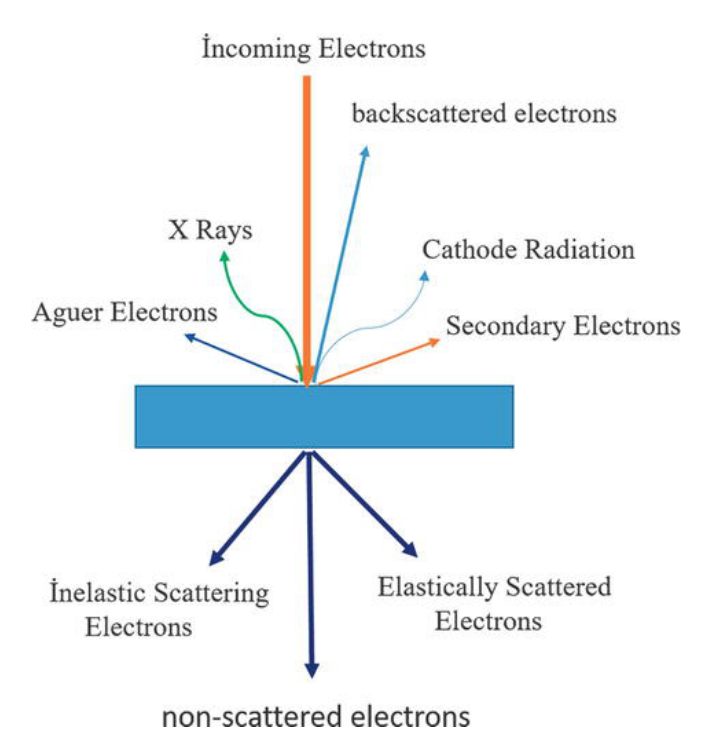


Figure 2.8: Rays and electrons formed as a result of the interaction of the incoming electron beam. [9]

In EDS analysis, the sample is hit with a beam of electrons inside the SEM. These electrons collide with the atoms in the sample and can knock out some of the electrons from the inner shells of those atoms. When this happens, an electron from a higher energy level (outer shell) moves in to fill the empty spot. As it does, it releases energy in the form of an X-ray. Each element gives off X-rays with specific energy values, like a signature.

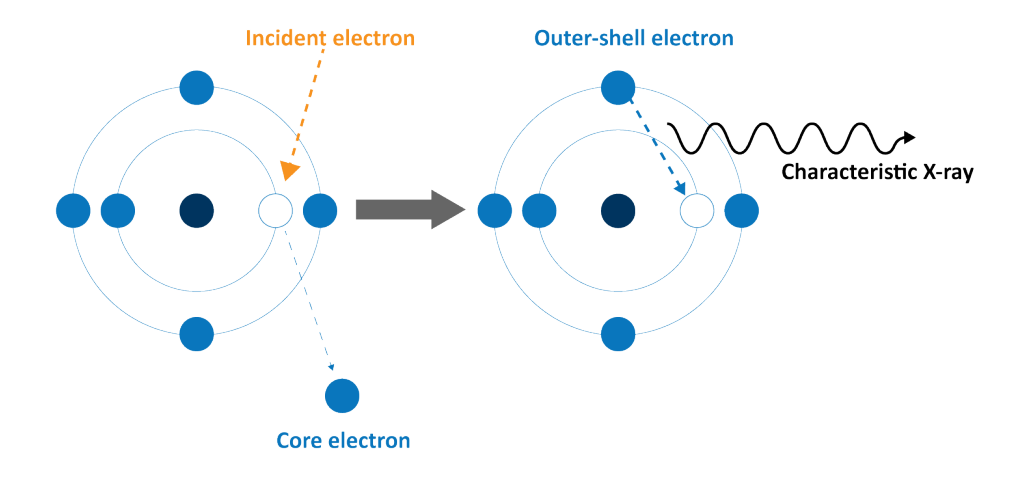


Figure 2.9: Characteristic X-ray emission from an atom. [10]

The X-rays given off by the sample are detected and measured using a Silicon Drift Detector (SDD). For each point on the sample, the detector records the energy and intensity of the X-rays. Special software, along with a database of known X-ray signals, is then used to figure out which elements are present based on the energy of the X-rays, and how much of each element is there based on the intensity. The result is an EDS spectrum—a graph that shows peaks at different energy levels. Each peak represents a specific element, and the taller the peak, the more of that element is in the sample.



Figure 2.10: JSM-7610FPlus Schottky Field Emission Scanning Electron Microscope.

2.3 Measurement System

We performed resistivity measurements with respect to temperature in our laboratory. For this, we used a current source, a voltmeter, a temperature controller, a chiller, and the Closed Cycle Refrigerator system (CCR). The complete setup of the measurement system is shown in the given figure.

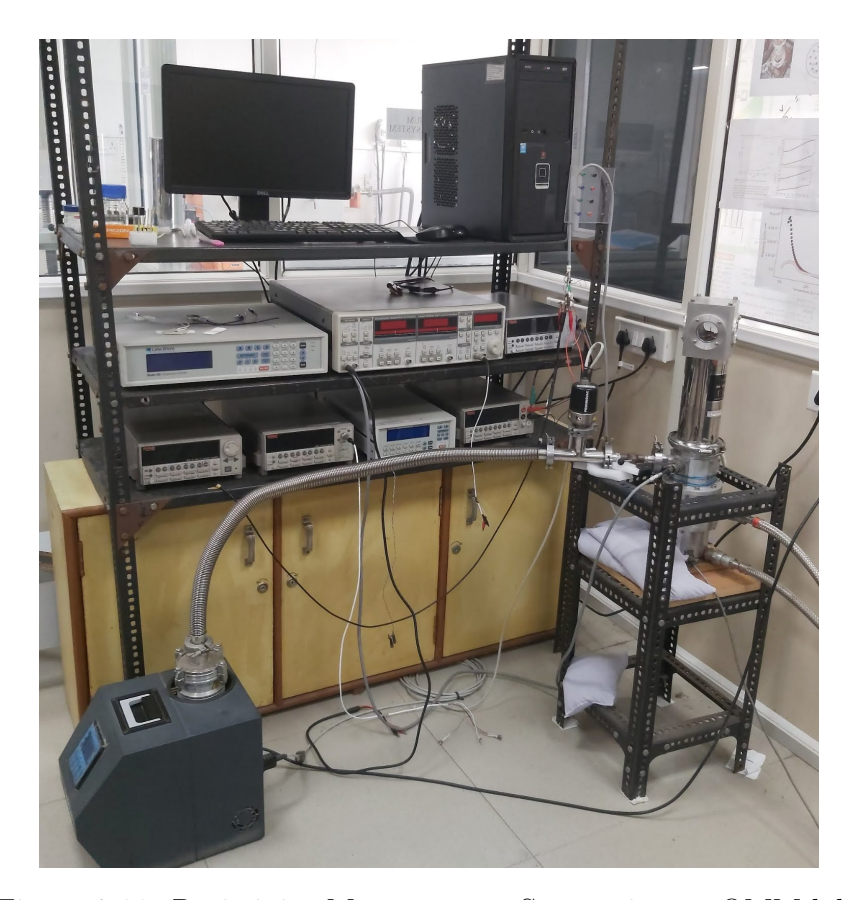


Figure 2.11: Resistivity Measurement System in our QMM lab.

2.3.1 Closed Cycle Refrigerator System

It is the Janis CCR system that we used for the resistivity measurements. It includes components like compressor for the supply of high pressure helium gas, a cold head which expands the helium gas to cool the sample, the gas lines that are connected between the compressor and cold head for the supply and return fittings, and transfer the helium gas between them. It also equipped with a radiation shield which is used to intercept room temperature radiation.

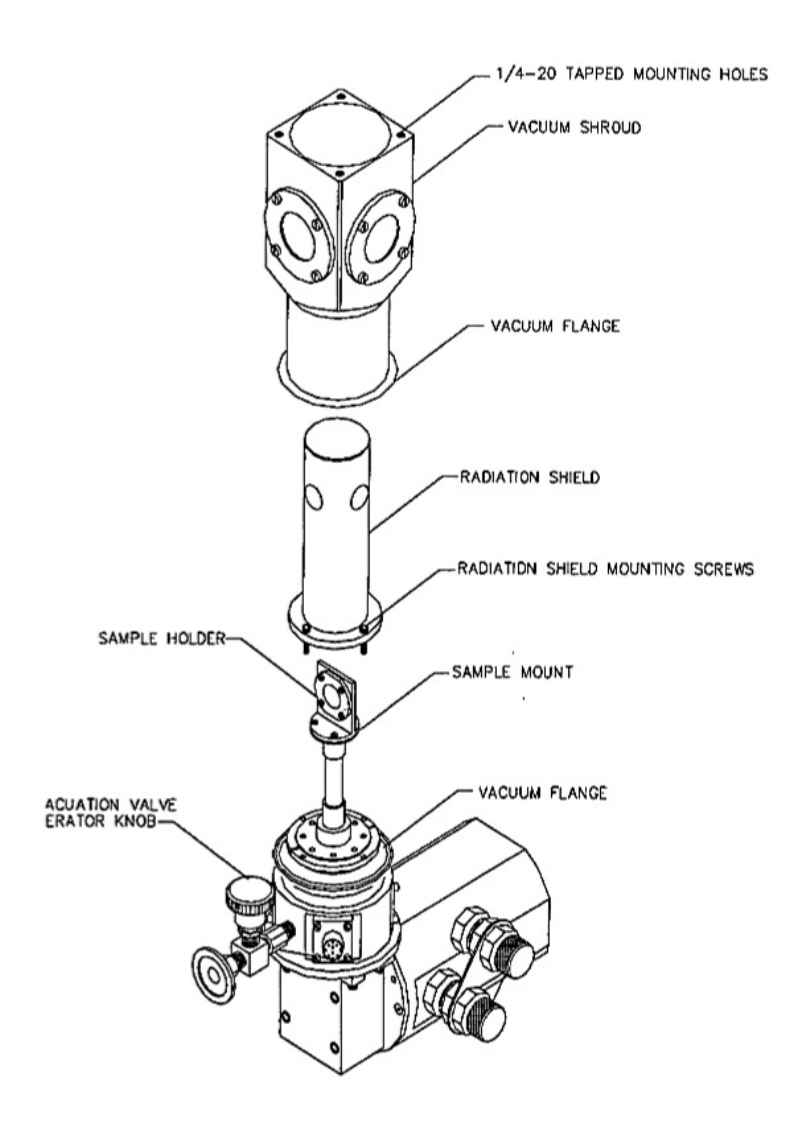


Figure 2.12: Schematic of the Janis CCR System.

Principles of Operation: The valve motor turns a rotating disc that controls the flow of helium gas. This high-pressure helium drives a back-and-forth (reciprocating) movement of the displacer inside the cylinder. Special ports in the valve disc are designed so that the displacer completes two full cycles for every turn of the disc. As the valve rotates, it directs helium through channels in the slack cap and into the regenerators. These regenerators—cooled during the previous exhaust phase—help lower the temperature of the incoming helium gas. As the cooled gas continues through the slack cap passages, it pushes the cap upward, which lifts the displacer. This movement creates space for the cooled gas to expand at the heat stations after it has passed through the regenerators. Simultaneously, as the displacer lifts, the gas above the slack cap is partially compressed and pushed through the orifice into the surge volume.

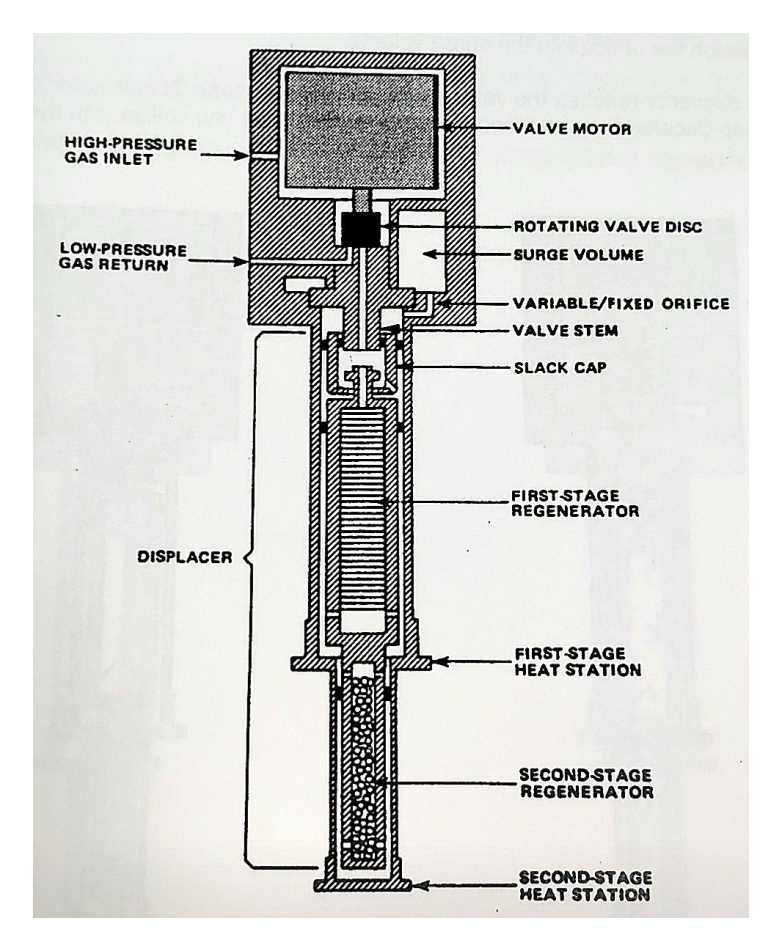


Figure 2.13: Schematic of the Cold Head.

Before the displacer reaches the valve stem, the valve shuts. At this point, the gas above the slack cap gets compressed, which slows down and stops the displacer, preventing it from hitting the valve stem. When the valve then opens for the exhaust phase, the high-pressure gas at the heat stations is allowed to expand. This expansion cools the heat stations, and the outgoing gas also helps cool down the regenerators. As the pressure drops, some of the partially compressed gas from the surge volume flows out, pushing the slack cap and displacer back toward the heat stations. This movement not only clears out the exhaust but also repositions the displacer before it reaches the heat stations again. As this cycle repeats, the temperature at the heat stations continues to drop, enabling refrigeration at cryogenic temperatures. [18]

2.3.2 Current Source

We used Keithley's Model 6221 AC and DC current source. The source provides us with a DC current from 0.1pA to 105mA with the voltage compliance limit from 0.1V to 105V in 10mV

steps. It consists of an analog filter to slow down output response and a banana jack guard output for the voltage measurements. It have features like Sweep functions (linear staircase, logarithmic staircase, and custom) and Waveform functions (sine, square, ramp and arbitrary function) for the desired output of current.

2.3.3 Voltmeter

We used Keithley's Model 2182A Nanovoltmeter. It has sensitivity upto 1nV to provide accurate ultra-low voltage measurements. For making accurate temperature measurements, it has a built-in thermocouple linearization and cold junction compensation. For low noise levels, it has just 15nV peak-to-peak noise t 1 s response time, with 40nV to 50nV peak-to-peak noise at 60 ms.

2.3.4 Temperature Controller

We used Lakeshore's Model 335 Temperature Controller. It operates down to 300 mK with appropriate NTC RTD sensors. Two configurable PID loops providing 50 W and 25 W or 75 W and 1 W. It supports diode, RTD, and thermocouple temperature sensors. It has an autotuning feature which automatically calculate PID control parameters which is useful for smooth functioning.

2.4 Physical Property Measurement System (PPMS)

It is an automated low-temperature and magnet system for the measurement of material properties like specific heat, magnetic AC and DC susceptibility and both electrical and thermal transport properties (like hall effect, magnetoresistance and seebeck effect). [19]

PPMS consists of an helium source that controls the sample's temperature and provides a range from 1.9 to 400 K. Also, it includes magnetic field which can go up to \pm 16 T.

The important hardware systems that PPMS includes are:

• **Dewar**: The dewar contains the liquid-helium bath in which the probe is immersed. Primarily constructed of aluminum, the outer layer of the dewar has reflective superinsulation to help minimize helium consumption.

- Baffled Rods: The probe contains rods that run along its entire length, which house the electrical connections for both the magnet and the impedance assembly. One of these rods also includes the helium-level meter. Multiple baffles are positioned along the probe to support and stabilize the rods.
- **Probe**: The probe is placed into a liquid-helium bath within the dewar. It's a complex device made up of sensitive components and includes key systems such as the temperature-control hardware, a superconducting magnet, a helium-level meter, gas lines, connectors for the sample puck, and various electrical connections.
- Magnets: The magnet is a superconducting solenoid made from a niobium—titanium alloy embedded in copper. It is positioned on the outside of the probe, ensuring it remains constantly immersed in liquid helium.



Figure 2.14: Image of an PPMS.

Chapter 3

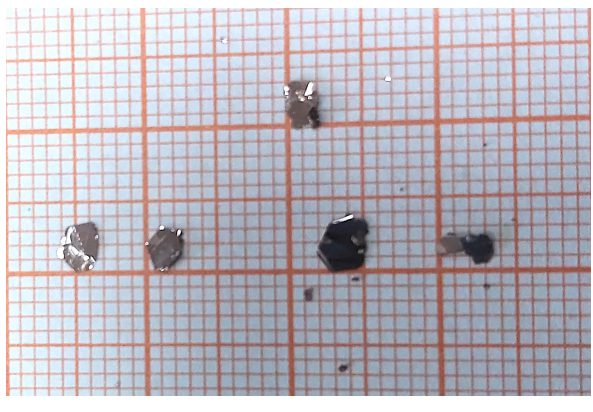
Characterization Results

In this chapter, we will talk about the results we obtained from the characterization techniques mentioned above.

3.1 Material : $TiSe_2$

3.1.1 Synthesis of Single Crystals by CVT Method

TiSe₂ was synthesized by mixing ultrapure Ti, Se, and I₂ (5.0 mg total) in a suitable ratio and sealing the mixture in a quartz ampule under vacuum ($<1.5 \times 10^{-4}$ mbar). The ampule was heated in a two-zone furnace (650 °C hot end, 550 °C cold end) for 14 days, then cooled to room temperature at 30 °C/h.



(a) Experimental



(b) Micro-images of crystals

Figure 3.1: Images of single crystal of TiSe₂ grown in our LTP lab.

3.1.2 Synthesis of Polycrystalline by Solid State Method

We prepared two samples of polycrystalline TiSe₂ for studying the material's sensitivity towards synthesis process.

First procedure: The polycrystalline TiSe₂ sample was synthesized in two steps. First, Ti and Se powders were mixed in the appropriate stoichiometric ratio, sealed in a quartz ampoule, and heated in a muffle furnace at 650 °C for 24 hours with a ramp rate of 120 °C/h. The resulting product was then ground again, resealed, and subjected to a second heat treatment at 950 °C for 48 hours with the same ramp rate. Afterward, the sample was cooled to 650 °C at 2 °C/h, held at this temperature for 24 hours, and finally cooled to room temperature.

Second procedure: The elements Ti and Se were mixed in appropriate ratio and sealed. Then the ampoule was loaded into the muffle furnace for 7 days at 800 °C at a rate of 5 °C/min from room temperature to 800 °C. After 7 days, material was cooled from 800 °C to the room temperature at a rate of 30 °C/h.



Figure 3.2: Polycrystal sample of TiSe₂

3.1.3 XRD pattern, Raman Spectra and EDS data of TiSe₂

• The PXRD pattern confirms that the TiSe₂ sample synthesis is crystallized in a trigonal crystal structure with a space group P -3 m 1 (164). No XRD peak corresponding to any impurity peak is detected. All major peaks: (001), (002), (003), and (004) are present in

the obtained pattern.

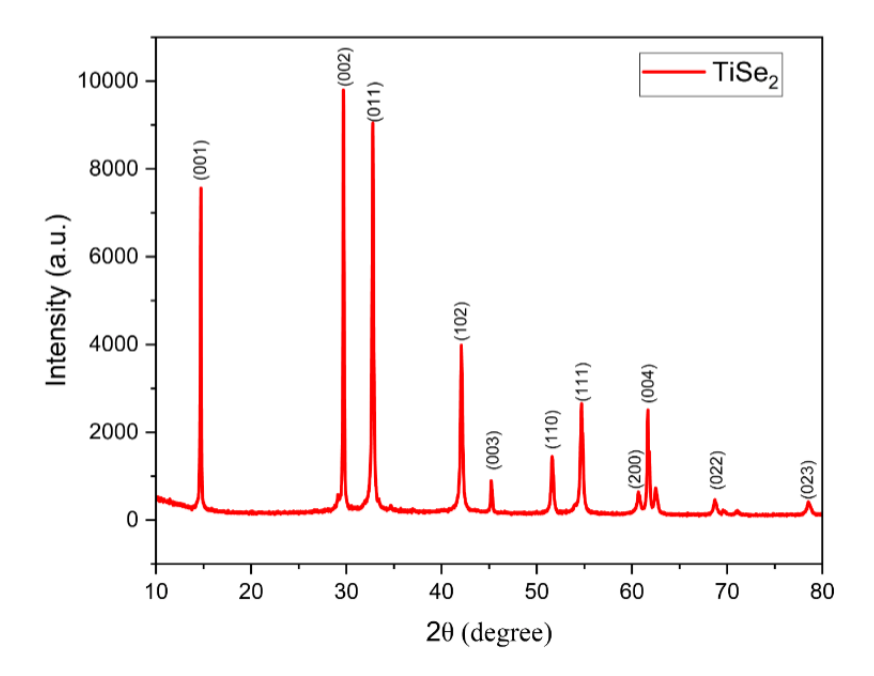


Figure 3.3: XRD pattern of TiSe₂.

• Raman vibration modes are observed at 136 cm⁻¹ and 198 cm⁻¹ respectively acquired with $\lambda = 633$ nm. These vibrational modes are identified as A_{1g} and E_g modes of TiSe₂ and are in accordance with the previous report on 1T phase of TiSe₂.

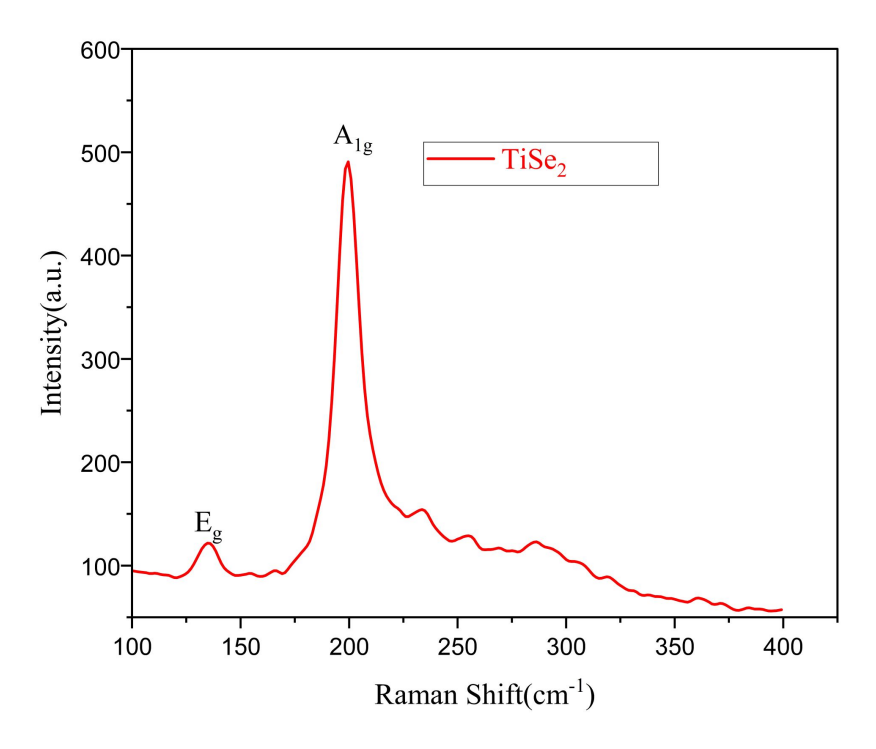


Figure 3.4: Raman spectra of TiSe₂.

• We also perform the EDS on our samples and the data of our sample TiSe₂ clearly shows the composition of elements Ti and Se to be in accordance with the stoichiometry.

Table 3.1: EDS Analysis Results

Element	Atomic (%)	elemental ratio		
Titanium (Ti)	33.3	1		
Selenium (Se)	64.3	1.93		
Iodine (I)	2.4	0.07		

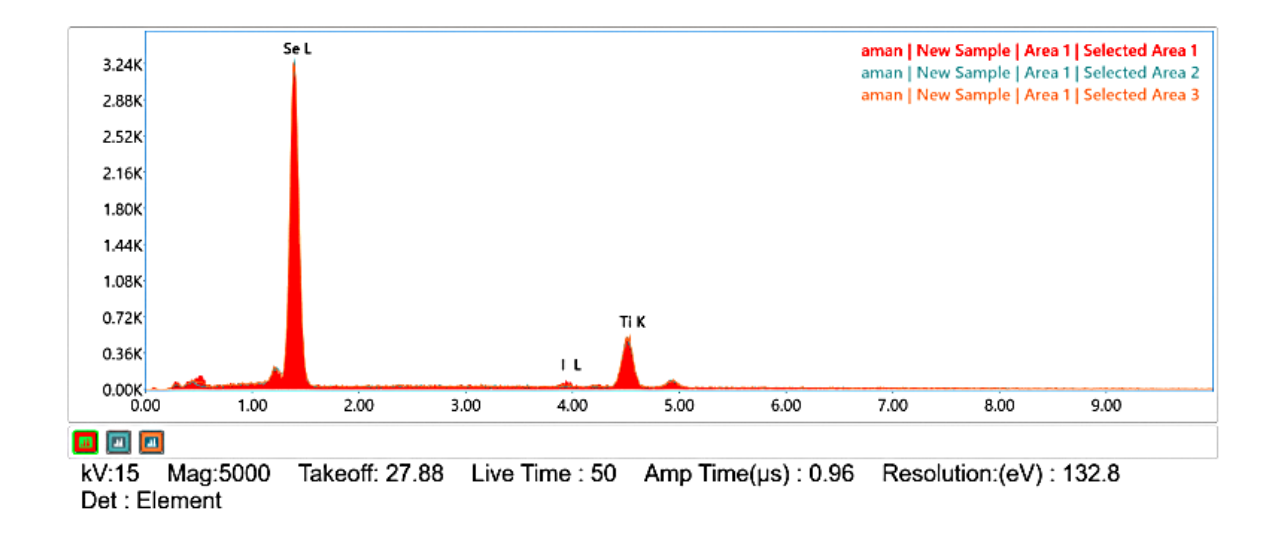


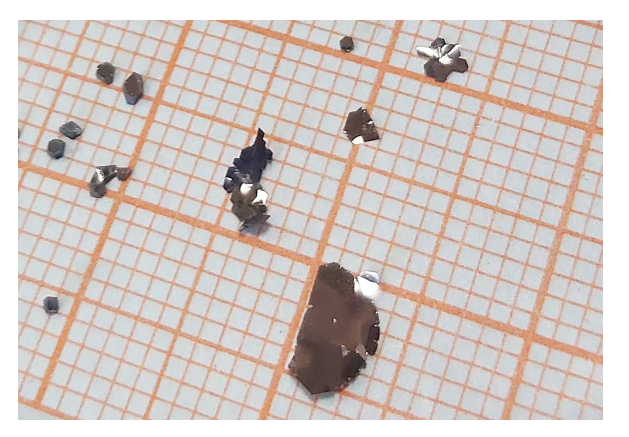
Figure 3.5: Chemical Composition of TiSe₂.

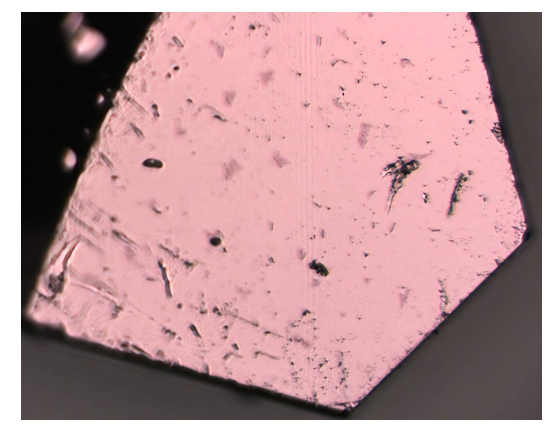
3.2 Material : $\mathbf{Zr}_{0.05}\mathbf{Ti}_{0.95}\mathbf{Se}_{2}$

3.2.1 Single Crystals by CVT Method

The single crystals were synthesized in two steps. First, we prepared a polycrystalline sample of $Zr_{0.05}Ti_{0.95}Se_2$ by taking pure elements of Ti, Zr, and Se in their stoichiometric ratio. The elements were mixed in an inert atmosphere in a glove box and then the mixture were shaped into a pellet using hydraulic press. The pellet then sealed in a quartz tube and placed in a muffle furnace for 24 h at 650 °C at a rate of 120 °C/h. Then the obtained pre-reacted powder was grounded again and heated to a higher temperature of 950 °C at a rate of 120 °C/h for 48 h. Then the sample cooled to 650 °C with rate of 2 °C/h and then kept at 650 °C for 24 h. Then it was finally cooled to room temperature at a rate of 30 °C/h. In the second step, the

polycrystalline sample was sealed in a quartz tube and placed in a two-zone furnace for 6 days. The hot end temperature was kept at 750 °C and the cold end temperature at 600 °C. After six days, the material cooled to room temperature at a rate 30 °C/h.





(a) Synthesized single crystals

(b) Microscopic image of single crystals

Figure 3.6: Images of single crystal of $Zr_{0.05}Ti_{0.95}Se_2$ grown in our LTP lab.

3.2.2 XRD pattern, Raman Spectra and EDS data of $Zr_{0.05}Ti_{0.95}Se_2$.

The XRD, Raman, and EDX data of $Zr_{0.05}Ti_{0.95}Se_2$ matched with the reference data which confirms its high quality and good structure.

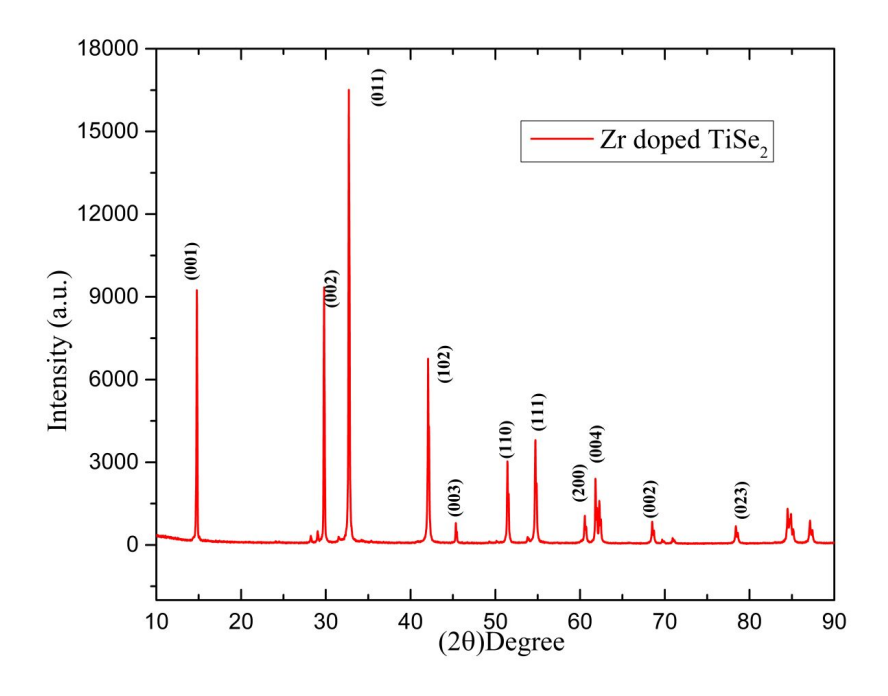


Figure 3.7: XRD pattern of Zr_{0.05}Ti_{0.95}Se₂.

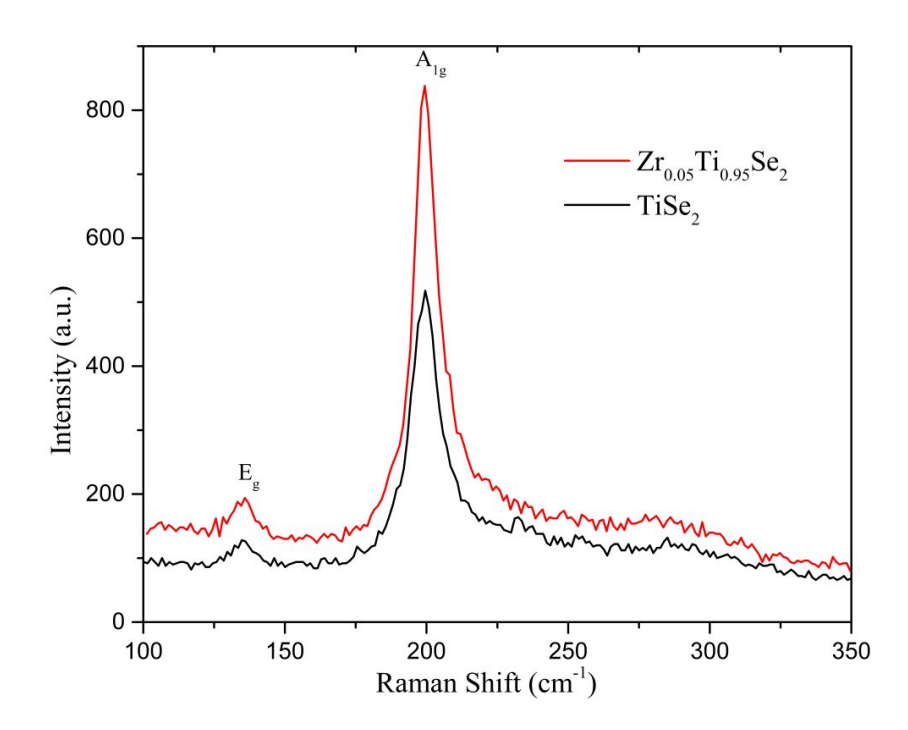


Figure 3.8: Raman spectra of $Zr_{0.05}Ti_{0.95}Se_2$ compared with the raman spectra of $TiSe_2$.

EDAX APEX

	aman								
eZAF Quar Element	nt Result - Anal Weight %	ysis Unc	ertainty: 6.94 Atomic %	% Error %	Net Int.	R	Α	F	
Ti K	25.1	0.78	35.8	5.4	89.2	0.8713	0.8992	1.0324	
Se L	69.8	2.29	60.4	6.3	289.3	0.8119	0.5780	1.0017	
7r I	5.1	1.37	3.8	22 1	11.2	0.8296	0.4878	1.0030	

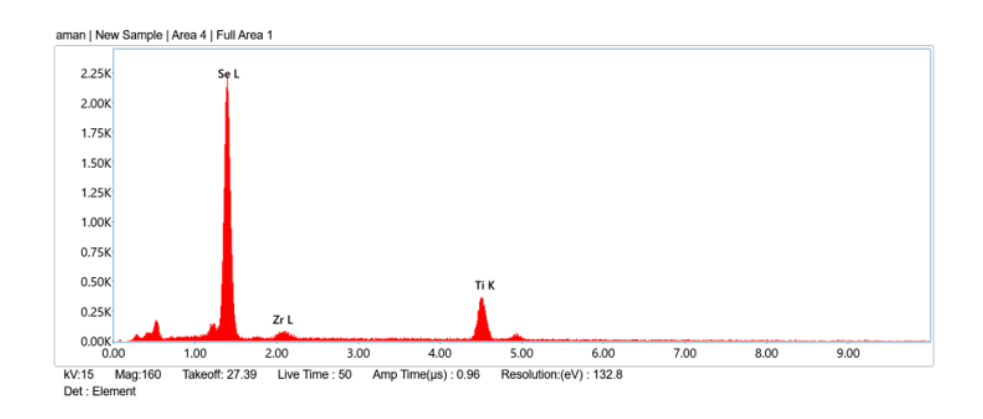


Figure 3.9: Chemical composition of $\rm Zr_{0.05}Ti_{0.95}Se_2$.

Chapter 4

Electronic Properties

In this chapter, we discussed the electronic properties of 2D materials we prepared in our lab. These are the properties we observed during the different measurements we performed on our samples. These measurements helped us to understand the transport properties of these materials and gave us the detailed information about their behavior in response with their surroundings.

4.1 Material : $TiSe_2$

4.1.1 Introduction

Titanium Diselenide (TiSe₂) is a 2D material and belongs to the TMDC family. It is one of the most studied materials among other TMDCs. In 1976, Di Salvo et al. reported a $(2 \times 2 \times 2)$ commensurate CDW transition at 200 K accompanied by a periodic lattice distortion. It is still an ongoing debate on the possible reason for the occurrence of CDW. It's electronic band structure generally fluctuate between semimetal and semiconductor as in many research papers, it has been reported that it is a semimetal but recent ARPES data confirms a bandgap of 74 meV which denies its semimetal nature. The resistivity measurement of TiSe₂ has been important to determine the CDW transition temperature and the Metal-Insulator Transition. TiSe₂ has been very sensitive to its growth conditions and dilute impurities. Different growth conditions can affect its crystal structure and can change the transport properties. We prepared both single crystal and polycrystal samples of TiSe₂ to study the transport properties.

4.1.2 Resistivity vs Temperature Measurement

The ρ -T measurements of the polycrystalline samples clearly show the dependence of the material's properties on the synthesis conditions.

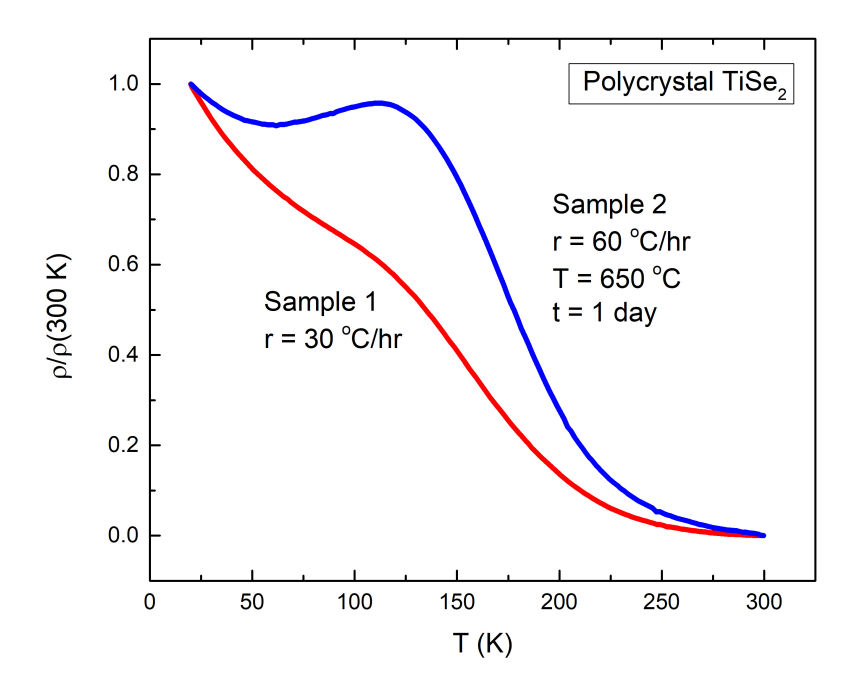


Figure 4.1: ρ -T plot of polycrystalline samples of TiSe₂. Here, red line and blue line represents sample 1 and sample 2 respectively.

The properties of TiSe₂ depend on the Postsynthesis cooling rate (r), Postsynthesis annealing time (t), and Postsynthesis annealing temperature (T). It has been reported that slow cooling rate and postsynthesis annealing can improve the quality of crystals by relieve microstrain and increase grain size. hence, any change in these three quantities can significantly change the properties. We prepared two polycrystal samples with different growth conditions shown in figure 3.5. In first sample, we cooled the sample at a rate of 30 °C/h and did not perform any annealing process. In second sample, we made the annealed for 1 day at a temperature of 650 °C and then cooled it at a rate of 60 °C/h. Due to these changes we can observe notable changes in the properties of these two samples. The peak position is similar in both but the hump of peak in second sample is greater as compared to the first sample. Though both the samples show semiconducting behavior but the values of resistivity differs in both. [13]

Fig. 3.7 shows ρ -T measurements result of single crystal TiSe₂. The properties of single crystals are quite different than those seen in the polycrystalline sample.

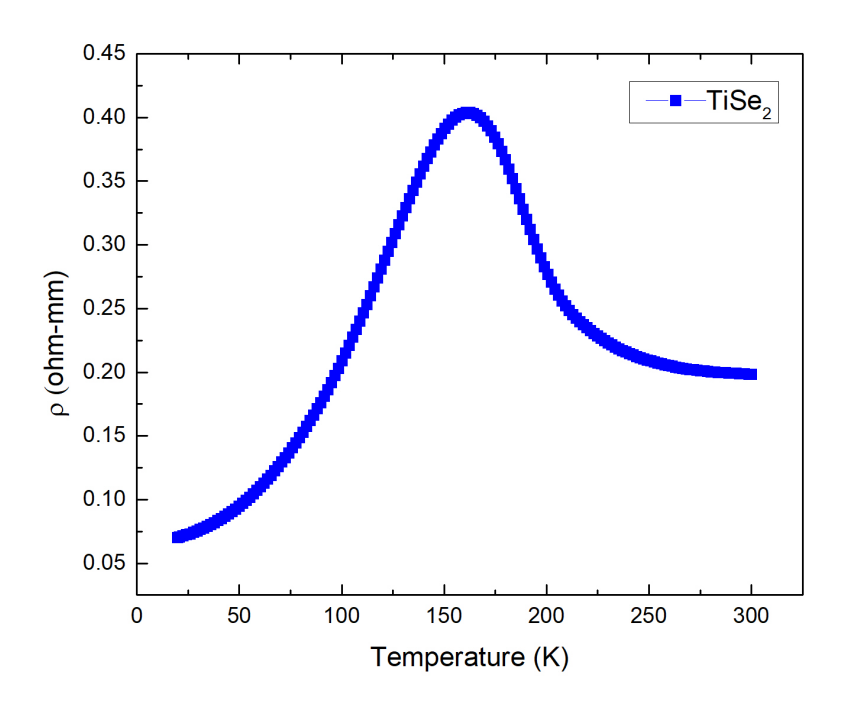


Figure 4.2: ρ -T plot of TiSe₂ single crystal.

In single crystals, at low temperature, the resistivity shows metallic behavior and not semiconducting which is the case for polycrystalline. The possible reason behind this can be the transporting agent (Iodine) that was required for the growth of single crystals. Iodine can possibly substitute Selenium (Se) atoms partially and dope the system. Also the deficiency of Selenium serves as a method of self-doping and, hence, due to these reasons, there have been an additional density of states near fermi surface that can enhance the conductivity on cooling.

In fig. 3.7, we can observe a clear peak around 160 K which can possibly due to the temperature-dependent thermal populations of 2D holes and 3D electron bands and not because of the charge density wave, which is reported in many research papers. In fig. 3.8, the minimum of $d\rho/dT$ represents the CDW phase transition which is ~ 185 K. [14]

CDW transitions are often explained by Fermi surface nesting, but in TiSe₂, this does not apply because both the normal and CDW phases have a bandgap, which means that there is no nesting. The bandgap actually becomes larger with the (2×2) distortion, which happens because the conduction band's degeneracy is lifted, indirectly affecting the valence bands. This

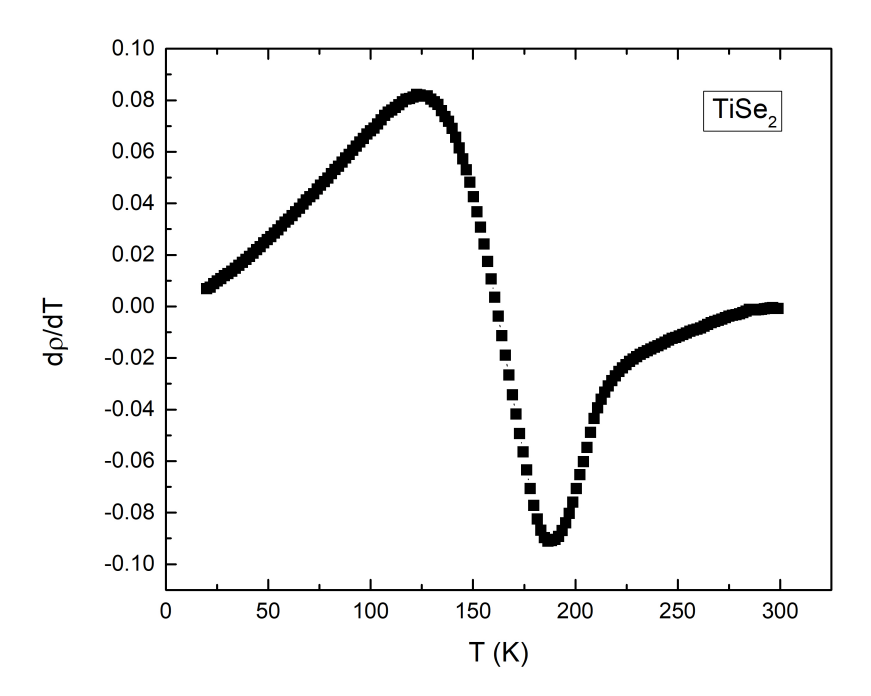


Figure 4.3: The derivative of the resistivity plotted as a function of temperature.

bigger gap pushes the occupied Se 4p states to lower energies, which initially reduces the total energy. However, this effect is eventually offset by other factors, like an increase in elastic energy.

Talking about temperature-dependent thermal populations, it had been confirmed by hall effect measurements of $\mathrm{TiSe_2}$, which clearly indicated a change in charge carriers as temperature rises. According to the data, at low temperatures, electrons are majority charge carriers that dominate the transport properties but as temperature rises, thermally activated hole-like carriers increase significantly and becomes majority charge carriers, affecting the properties of material and this change occurs around a characteristic temperature of $\sim 160~\mathrm{K}$.

4.2 Material : $\mathbf{Zr}_{0.05}\mathbf{Ti}_{0.95}\mathbf{Se}_2$

4.2.1 Introduction

Transition Metal Dichalcogenides (TMDCs) are one of the most studied materials among other 2D materials. They exhibit exceptional physical and chemical properties that make them suitable for almost all types of electronic applications. The properties of TMDCs can be modified easily

through intercalation or by substituting transition metal or chalcogen atoms. Material like TiSe₂ are one of the most studied materials and many studies are there on the intercalation or substitution of other transition metals (Mn, Cr, Pd or Fe) replacing Titanium, but there are only a few studies on the zr doped TiSe₂. So we try to synthesis zr doped TiSe₂ in which we replace 5 at.% Ti by Zr to observe the impact of the substitution on the properties such as charge density wave and metal-insulator transition.

4.2.2 Resistivity vs Temperature Measurement

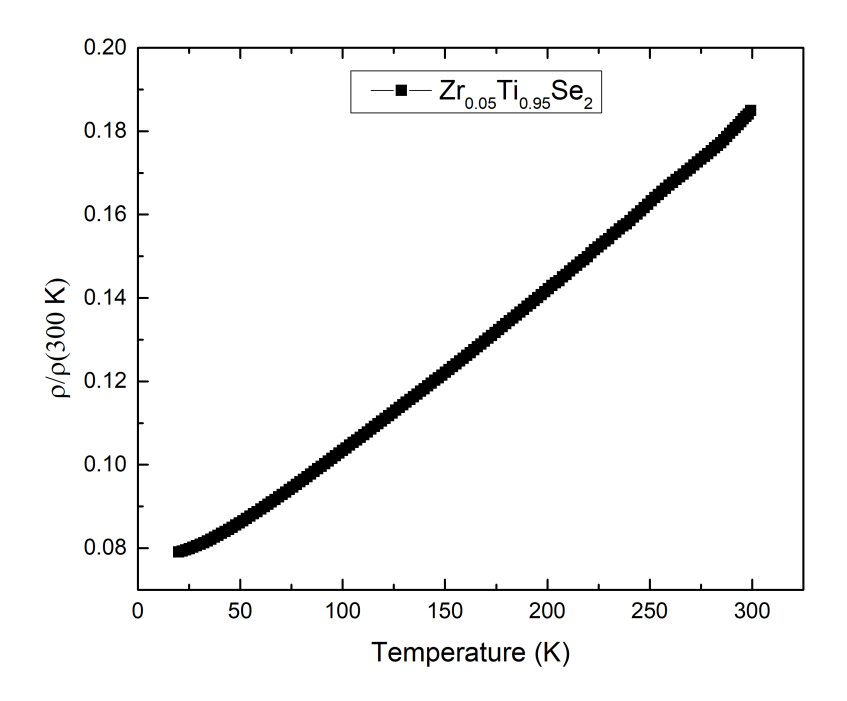


Figure 4.4: Resistivity Measurement of Zr_{0.05}Ti_{0.95}Se₂ polycrystalline sample.

We carried out the resistivity measurement of polycrystal Zr_{0.05}Ti_{0.95}Se₂. We observed that the material shows a metallic-type behavior from high temperature to low temperature, which is different from pure TiSe₂. Substitution of Ti by Zr can affect the binding energy of components which can result in fermi level shift also modifying the electronic structure. The energy of the Zr 4d orbital is considerably higher compared to the Ti 3d orbital, it can be expected that a Zr 4d – Ti 3d charge transfer will occur. As both the Zr 4d and Ti 3d bands are partially unfilled, they are expected to contribute to the formation of a conduction band in the compound. The

density of states (DoS) near the bottom of the conduction band is expected to decrease with the increased Zr concentration. This should increase the Fermi level for a constant conduction band electron concentration, thus increasing the binding energies of all electrons in material. [15]

4.2.3 MR(%) Vs Magnetic Field

To study the magneto-transport properties of Zr-doped TiSe₂, we measured its magnetoresistance with respect to magnetic field at different temperatures (10 K AND 300 K).

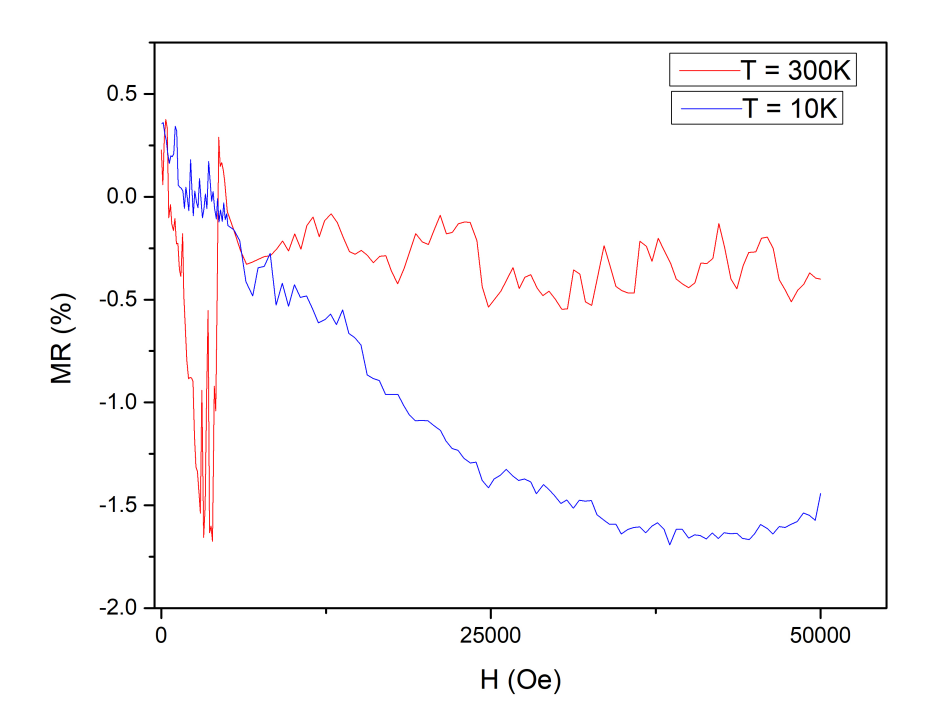


Figure 4.5: Magnetoresistance vs Magnetic field plot of $\rm Zr_{0.05}Ti_{0.95}Se_2$ at temperatures- 10 K and 300 K.

We analyzed this plot and we observed that at both the temperatures, the resistance of the material is negative which represents the negative MR. At low temperatures, around 10 K, we noticed that resistance values start to become more negative, which might be due to weak localization, a behavior that the parent material, TiSe₂, is known to show at low temperatures. Also, the resistance values of Temperature 300 K, at low magnetic fields, show a dip which can be inferred as a noise which can arise because of the connection break or some other reasons.

As compared with the parent material TiSe₂, the properties of Zr-doped TiSe₂ have similar traits and show similar kind of phenomenon at low temperatures. From this we can conclude

that the doping of Zr in TiSe₂, which had a strong impact on the resistivity causing noticeable changes in its behavior, also affected the MR data but not significantly and the phenomenons reported in TiSe₂ are still accountable for most of the properties in this material.

4.3 Material : ZrSe₂

4.3.1 Introduction

Zirconium diselenide (ZrSe₂) is a two-dimensional material that belongs to the transition metal dichalcogenide (TMDC) family. It is a semiconductor with an indirect band gap of approximately 1.2 eV and holds promise for applications in photovoltaic and thermoelectric devices. However, growing ZrSe₂ with precise stoichiometry is challenging, and deviations can introduce native defects. Unintentional n-type conductivity is often observed in ZrSe₂, which is generally attributed to excess Zr atoms acting as donors. In this study, we focus on how these defects significantly influence the transport properties of the material.

4.3.2 Resistivity vs Temperature Measurement

We study the transport properties of $ZrSe_2$ by performing measurements such as resistivity (ρ) vs temperature (T). The results of resistivity (ρ) vs temperature (T) measurements clearly indicate the metallic behavior, which is contrary to its nature as $ZrSe_2$ is a semiconductor with a indirect band gap of 1.2 eV. This behavior of $ZrSe_2$ can be understood by considering structural defects, ionized impurities or deviation of the elements from stoichiometry. Since it has been reported that the presence of additional Zr may result in the metallic characteristic of the material, so we performed EDS to find out the composition of elements in our sample, and the data confirmed the presence of additional Zr (3 at.%) in our samples. The resistivity varies linearly with temperature at higher temperatures between 200 K to 300 K, which responds to the signature of electron-phonon scattering. To confirm the type of scattering in $ZrSe_2$, we performed curve fitting of our data. Hence, for the resistivity above 200 K, the data is fitted to the expression

$$\rho(T) = A + BT \tag{4.1}$$

where, A and B are the fitting parameters.

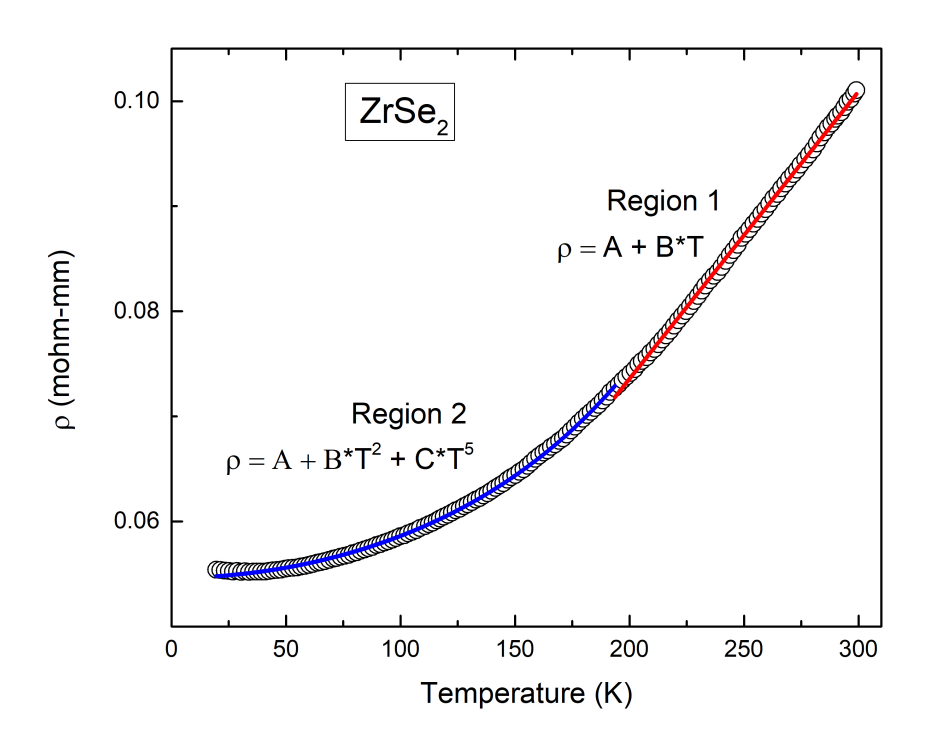


Figure 4.6: Resistivity (ρ) vs Temperature (T) plot of ZrSe₂. The red line is fitted to Eq. (4.1) and the blue line is fitted to Eq. (4.2).

Below 200 K, the resistivity does not vary linearly with temperature because the electronphonon scattering becomes weak as the temperature starts decreasing and turn out to be a T^5 dependence on temperature. At low temperatures, electron-electron scattering dominates, and the resistivity in this region is dependent as T^2 on temperature. So the data for this region is fitted to the expression

$$\rho(T) = \rho_0 + CT^2 + DT^5 \tag{4.2}$$

where, ρ_0 , C, and D are the fitting parameters. [16]

4.4 Material : $ZrSe_3$

4.4.1 Introduction

Zirconium triselenide (ZrSe₃) is a quasi-1D material belongs to the family of transition metal trichalcogenides (TMTCs). It is a semiconductor by nature with an indirect band gap of 1.1 eV. It exhibits a chain-like structure with linear chain of metal atoms parallel to the crystallographic b-axis, which is the growth axis. The crystal grow in the form of layers which run parallel to the b-axis. These layers are stacked along the c-axis by weak van der Waals bonds between the Se atoms. To study ZrSe₃, we synthesized the single crystals of it and did the measurements to examine the electronic properties of them.

4.4.2 Resistivity vs Temperature Measurement

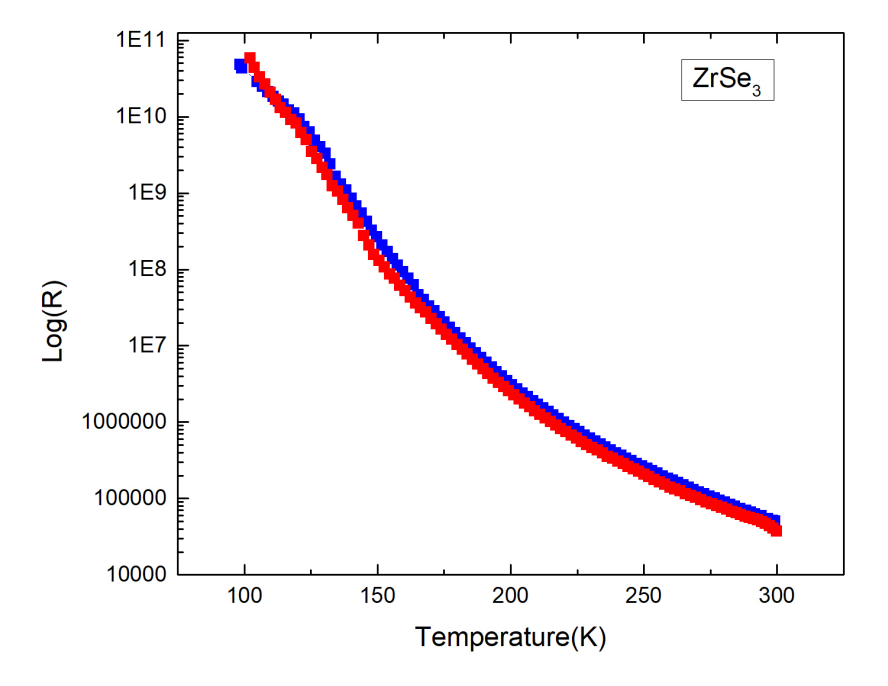


Figure 4.7: Resistivity (ρ) vs Temperature (T) plot of ZrSe₃. The red and blue lines represents the warming and cooling of samples during the measurement.

We conducted the measurement of resistivity vs temperature (ρ -T) of ZrSe₃ and the results clearly indicate its semiconducting behavior. Also, during the measurement process, we were

unable to use the four-probe on this material because of its high resistance values. So we tried to perform the measurement using the two probe system and it succeeded but still as the temperature decreased far low, the resistivity value went too high which makes it difficult for the system to measure further data.

From ρ -T plot, we analyzed that at low temperatures, ZrSe₃ begins to deviate from its semiconducting nature to the insulating behavior which was confirmed by our ρ -T plot. With decreasing temperature, the resistance of the material reaches so high values that we need to plot the resistance values in logarithmic form. The possible reason behind this behavior can be explained by considering the band gap between the conduction band and valence band and the energy required by charge carriers to travel between them. So, as the temperature starts decreasing, the energy required by the charge carriers to move from the valence band to the conduction band increases, which can result in a decrease of the conductivity and hence an increase in the resistivity of the material.

4.4.3 MR(%) Vs Magnetic Field

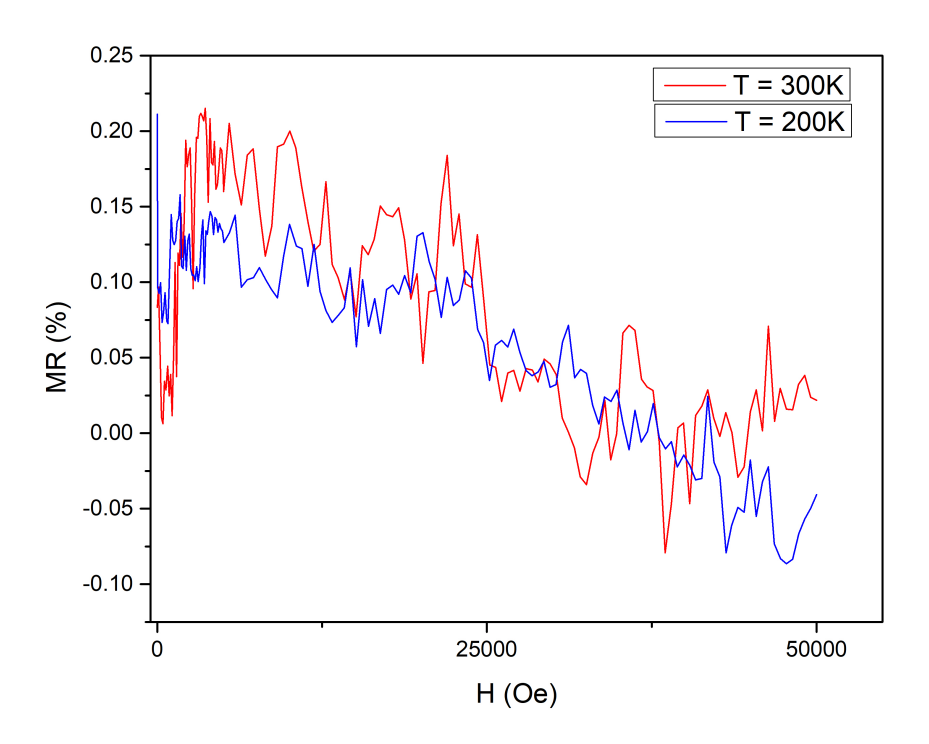


Figure 4.8: Magnetoresistance vs Magnetic field plot of ZrSe₃ at temperatures- 200 K and 300 K.

We carried out the measurement of magnetoresistance vs magnetic field to study the transport properties of ZrSe₃. From the analysis of the plot, we observed that there has been so much noise all over the range of magnetic field at both the temperatures. This possibly because of the low carrier concentration in the material which we concluded from its resistivity data, which clearly showed a transition from semiconducting to insulating nature. Also from the observation of plot, we inferred that the material showed a negative MR as the magnetic field values increased.

Chapter 5

Conclusion

In this work, we explored the magneto-transport properties of several two-dimensional (2D) materials, especially focusing on transition metal chalcogenides like TiSe₂, ZrSe₂, ZrSe₃, and Zr_{0.05}Ti_{0.95}Se₂. These materials are known for their interesting electronic behaviors, particularly under the influence of magnetic fields. Through our experiments, we were able to explore how these materials respond to various synthesis conditions and how their structural characteristics affect their electronic properties.

We used both single crystals and polycrystalline forms of the materials to examine their differences. For TiSe₂, we found that the sample's resistivity and overall behavior were highly sensitive to how the material was grown and cooled. For instance, the two polycrystalline samples showed a difference in their properties in resistivity vs temperature plot, which signifies the effect of synthesis on this sample, although the nature remains the same throughout. Also, at low temperatures, while polycrystalline samples, showed semiconducting behavior, the single crystal sample showed more metallic behavior. This change was likely due to the effect of synthesis parameters and the presence of iodine during the crystal growth of single crystal, which may have caused doping or changes in the electronic band structure.

We also observed a charge density wave (CDW) transition in TiSe₂, a phenomenon where the electron density becomes periodically modulated. Interestingly, our results suggest that this transition is not purely due to Fermi surface nesting, as seen in some materials, but may involve more complex interactions like changes in band structure and thermal effects. In the case of Zr_{0.05}Ti_{0.95}Se₂, where we replaced some of the Ti atoms with Zr, the material showed metallic behavior across all temperatures tested. This could be a result of changes in the energy levels of the Ti and Zr orbitals, leading to a shift in the Fermi level and alteration of the conduction band. The MR data showed weak localization phenomenon at low temperature and a negative MR as same as his parent material TiSe₂.

Similarly, ZrSe₂ showed an unexpected metallic character despite being a semiconductor by nature. After analyzing the material's composition, we found extra Zr atoms that may have acted as electron donors, thus making the material behave more like a metal. The fitting of resistivity data at different temperature ranges confirmed the dominant scattering mechanisms involved, including electron-phonon and electron-electron interactions.

Finally, ZrSe₃, which is a semiconductor, showed high resistance at low temperatures, indicating a transition from semiconducting to insulating behavior. This was most likely due to the increasing difficulty for charge carriers to move as thermal energy decreased. Also, its magnetoresistance values decreased with magnetic field and showed noise in the measurement, which possibly because of the small quantity of charge carriers.

Overall, this study highlights how sensitive 2D materials are to their environment, structure, and preparation methods. Even small changes in composition or synthesis can lead to significant differences in their electrical behavior. Understanding these effects is not only fascinating from a scientific point of view but also essential for designing future electronic and magnetic devices using these materials.

Bibliography

- [1] Singh, N.B. and Shukla, S.K. Properties of two-dimensional nanomaterials. In Two-Dimensional Nanostructures for Biomedical Technology (eds Khan, R. and Barua, S.) 73–100 (Elsevier, 2020).
- [2] Wikimedia Commons. Band Gap Comparison (2015).
- [3] Zhu, H. and Han, H. Charge density wave in low dimensional materials. J. Phys. Conf. Ser. 2338, 012028 (2022)
- [4] Hossain, M., Zhao, Z., Wen, W., Wang, X., Wu, J. and Xie, L. Recent advances in twodimensional materials with charge density waves: synthesis, characterization and applications. Crystals 7, 298 (2017).
- [5] Schmidt, P., Binnewies, M., Glaum, R. and Schmidt, M. Chemical vapor transport reactions—methods, materials, modeling. In Advanced Topics on Crystal Growth (ed. Ferreira, S. O.) 227–306 (InTech, 2013).
- [6] Berger, M., Yang, Q. and Maier, A. X-ray imaging. In Medical Imaging Systems: An Introductory Guide (eds Maier, A., Steidl, S., Christlein, V. and Hornegger, J.) 119–145 (Springer, 2018).
- [7] Ismail, K. Fabrication and characterisation of SERS substrates through photo-deposition of gold nanoparticles. Postgraduate Diploma Thesis, Abdus Salam International Centre for Theoretical Physics (ICTP), Trieste, Italy (2015).
- [8] Regonini, D. Anodised TiO₂ Nanotubes: Synthesis, Growth Mechanism and Thermal Stability. PhD thesis, University of Bath (2008).

- [9] Temiz, C. Scanning Electron Microscopy. In Scanning Electron Microscopy Applications and Advances (ed. Temiz, C.) (IntechOpen, 2022).
- [10] Nanoscience Instruments. Why EDS matters: The role of energy dispersive X-ray spectroscopy in materials science. Nanoscience Instruments Blog (2023).
- [11] Dresselhaus, M. S. Solid State Physics: Part I Transport Properties of Solids. Massachusetts Institute of Technology (2001).
- [12] Chen, Y. et al. Emulating weak localization using a solid-state quantum circuit. Nat. Commun. 5, 5184 (2014).
- [13] Moya, J. E. M. et al. Effect of synthesis conditions on the electrical resistivity of TiSe₂. Phys. Rev. Mater. 3, 084005 (2019).
- [14] Watson, M. D., Beales, A. M. and King, P. D. C. On the origin of the anomalous peak in the resistivity of TiSe₂. Phys. Rev. B 99, 195142 (2019).
- [15] Merentsov, A. I. et al. Isovalent substitution-induced pseudodoping in $Zr_xTi_{1-x}Se_2$ transition metal dichalcogenides. J. Chem. Phys. 162, 044704 (2025).
- [16] Ghosh, B. et al. Structural and electronic phase transitions in TiSe₂ at high pressure. Phys. Rev. B 106, 104102 (2022).
- [17] Anisotropic magnetoresistance (AMR) of Permalloy. Wikimedia Commons.
- [18] Janis Research Company. Janis Closed Cycle Refrigerator System Manual. Applied Cryogenics.
- [19] Quantum Design Inc. Physical Property Measurement System (PPMS).